Icarus **154**, 296–312 (2001)
doi:10.1006/icar.2001.6716, available online at http://www.idealibrary.com on IDEAL®

# Viscosity in a Dense Planetary Ring with Self-Gravitating Particles

Hiroshi Daisaka

*Department of Earth and Planetary Sciences, Faculty of Science, Tokyo Institute of Technology, 2-12-1 Ookayama, Meguro, Tokyo 152-8551, Japan; and Department of Astronomy, Graduate School of Science, University of Tokyo, 7-3-1 Hongo, Bunkyo-ku, Tokyo 113-0033, Japan*
E-mail: hdaisaka@geo.titech.ac.jp, daisaka@astron.s.u-tokyo.ac.jp

Hidekazu Tanaka

*Department of Earth and Planetary Sciences, Faculty of Science, Tokyo Institute of Technology, 2-12-1 Ookayama, Meguro, Tokyo 152-8551, Japan*

and

Shigeru Ida

*Department of Earth and Planetary Sciences, Faculty of Science, Tokyo Institute of Technology, 2-12-1 Ookayama, Meguro, Tokyo 152-8551, Japan*

Received February 29, 2001; revised June 22, 2001

**We have investigated the viscosity (the angular momentum flux) in dense, self-gravitating particle disks such as Saturn's main ring, by performing local *N*-body simulations. Viscosity could play important roles in evolution and structure formation of planetary rings. The ring's viscosity has been investigated with both theoretical and numerical approaches (e.g., Goldreich and Tremaine, 1978, *Icarus* 34, 227–239; Wisdom and Tremaine, 1988, *Astron. J.* 95, 925–940). However, these studies mainly considered systems including physical collisions of particles but not mutual gravitational interactions. Local *N*-body simulations by Salo (1995, *Icarus* 117, 287–312) and Daisaka and Ida (1999, *Earth, Planet Space* 51, 1195–1213) showed that a wake-like structure and clumps of particles are formed by the self-gravitational instability and that in such situations coherent motion of particles is dominant rather than random motion, which leads to an increase in radial velocity dispersion of particles. The wake structure and associated coherent motion are considered to affect the ring viscosity significantly.**

**Our simulation in this paper shows that the viscosity is strongly enhanced by the wakes. When the wake structure strongly develops, the coherent motion considerably enhances the translational viscosity, which was usually referred to as a local component in previous studies, and the effective viscosity is dominated by both gravitational torque due to the wake structure and the enhanced translational viscosity. We also find that in the presence of the wakes, the viscosity $\nu$ is given as $\nu \simeq C G^2 \Sigma^2 / \Omega_0^3$, where $G$, $\Sigma$, and $\Omega_0$ are the gravitational constant, the surface mass density of a ring, and the angular velocity, respectively. The non-dimensional correction factor $C$ depends on the distance from the central planet. For example, $C \simeq$ 6–20 for Saturn's B-ring. The effects of the enhanced viscosity on the structure and evolution of Saturn's main ring are also discussed.** 

*Key Words:* **planetary rings; Saturn.**

## 1. INTRODUCTION

Disk viscosity, which is related to angular momentum transport, would regulate evolution and structure formation of disk systems such as planetary rings (e.g., Lynden-Bell and Kalnajs 1972, Goldreich and Tremaine 1978b). The viscosity in a planetary ring has been studied with several approaches: analytical studies based on the Boltzmann equation (e.g., Goldreich and Tremaine 1978a, Borderies *et al*. 1985, Araki and Tremaine 1986), numerical studies with many particle simulations in rectangular local coordinates, including inelastic collisions (Wisdom and Tremaine 1988, Salo 1991, 1992a, Richardson 1994, Mosqueira 1996), and kinetic models based on a numerical algorithm that follows the evolution of velocity distribution (Greenberg 1988, Petit and Greenberg 1996).

In these studies, the viscosity was computed mainly through two components of momentum transport. One is the local component, which comes from momentum transport due to random motion of particles such as molecular viscosity. In the local component, the momentum is transported by transfer of the particle itself. Since particles have finite sizes, during a collision, momentum is also transported between the centers of the colliding particles without transfer of the particles. This non-local component plays an important role in such a dense particle system where the physical size of particles is comparable with the mean free path between successive collisions. To evaluate the viscosity, Goldreich and Tremaine (1978a) considered only the local component of the viscosity, whereas Araki and Tremaine (1986) included the non-local component. Wisdom and Tremaine (1988) examined these components of the viscosity with many particle simulations. The obtained total viscosity is an increasing



0019-1035/01 $35.00

function of optical thickness (depth) $\tau$, which does not satisfy the condition for the viscous instability proposed to explain axisymmetrical ringlet structures (Lin and Bodenheimer 1981, Lukkari 1981, Ward 1981).

However, as we will show later, momentum transport due to self-gravitational interactions is also important. Borderies *et al.* (1985) considered the transport due to self-gravity in the streamline model. In this paper, we hereafter refer to the "local" and "non-local" components as the "translational" and "collisional" components, respectively, because we will use the "local" for another concept. We call the transport due to self-gravity the gravitational component.

Local particle simulation first done by Wisdom and Tremaine (1988) has been extended to take into account self-gravitational interactions between particles by several authors (e.g., Salo 1992b, 1995, Richardson (1994), Daisaka and Ida 1999, Ohtsuki and Emori 2000). The local $N$-body simulations demonstrated the spontaneous formation of an inhomogeneous wake structure, which is induced by the effects of both self-gravity and collisional damping of particles. An increase in the disk surface density reduces the Toomre's parameter, $\mathcal{Q}$, of the gravitational instability given by (Toomre 1964)

$$\mathcal{Q} = \frac{\Omega_0 \sigma_r}{3.36 G \Sigma}, \tag{1}$$

where $\sigma_r$ is the radial velocity dispersion of ring particles, $G$ is the gravitational constant, $\Omega_0$ is the angular velocity, and $\Sigma$ is the surface mass density of a ring. Results of the $N$-body simulations indicate that the wake is formed when $\mathcal{Q} \lesssim 2$. Salo (1995) and Daisaka and Ida (1999) also showed that particles move no longer randomly but coherently in the wakes. Such coherent motion yields systematic motion with large bulk velocity, being $\mathcal{Q} \simeq 2$ for larger surface density. The wakes in simulations have a pitch angle of $\sim$20 degrees and the typical radial scale is almost equal to the longest wavelength, $\lambda_{\rm cr}$, of the axisymmetric instability mode (Julian and Toomre 1966) given by

$$\lambda_{\rm cr} = \frac{4\pi^2 G \Sigma}{\Omega_0^2}. \tag{2}$$

For the parameters of the Saturn's rings, the radial scale is on the order of $\sim$100 m.

In previous studies, the viscosity is evaluated only for disks in which particles are distributed uniformly in space but not for disks with the wakes described above. The wakes are expected to enhance angular momentum transport through the gravitational torque (Larson 1984) and the (turbulent) wake motion (Lin and Pringle 1987). Richardson (1994) calculated the ring viscosity with the results of local $N$-body simulations. He also showed gravitational wakes in simulations with size distribution of particles. However, in his calculations for evaluation of viscosity, the simulation region was so small that the wake structure was suppressed. Furthermore, the gravitational component of the angular momentum transfer was not considered in his simulations.

Petit and Hénon (1987a, 1987b, 1988) have investigated evolution of planetary rings as a three-body problem, taking into account both effects of the self-gravity and inelastic collisions of particles. Using the results obtained from the analytical and numerical approaches, they also constructed a kinetic model of the evolution of rings and did Monte Carlo simulations. In their model, a system evolves by cumulative effects of successive, independent pairwise interactions of particles. Such a treatment is valid for systems with small optical depth like Saturn's C-ring. However, in Saturn's A- and B-ring with optical depth $\tau \gtrsim 1$, collective effects would be rather important because of the wake formation due to the self-gravitational instability (e.g., Salo 1995, Daisaka and Ida 1999).

Angular momentum transport enhanced by the gravitational instability was investigated in gaseous accretion disks by $N$-body simulation with self-gravitating particles (Anthony and Carlberg 1988), SPH-simulation (Laughlin and Bodenheimer 1994), and hydrodynamical simulation (Laughlin and Rozyczka 1996). In these studies, basically, viscosity is evaluated through comparison with the solution of the diffusion equation. These results could not directly apply for a planetary ring system, because the accretion disk does not include the collisional effects. Moreover, detailed transport processes were not clear in these studies because only total angular momentum transport was discussed.

Takeda and Ida (2001) have investigated angular momentum transport of particle disks within the Roche limit to give physical insight into the results of lunar accretion by $N$-body simulations (Ida *et al.* 1997, Kokubo *et al.* 2000), in which a protomoon quickly formed from a proto-lunar disk made by a "giant impact" (Hartman and Davis 1975, Cameron and Ward 1976). Takeda and Ida (2001) formulated the angular momentum transport, using the Boltzmann equation. They divided the angular momentum flux into the translational, collisional, and gravitational components and calculated them directly from the results of their global $N$-body simulations with up to $10^5$ particles. In their formulations, the translational and collisional components are the same as those of Wisdom and Tremaine (1988).

In this study, we investigate the viscosity in a dense self-gravitating planetary ring with wakes. We calculate the viscosity (translational, collisional, and gravitational components), directly from the results of local $N$-body simulations, using the formulation by Takeda and Ida (2001). We focus on planetary rings like Saturn's ring, where the disk mass is small compared with the central planet (e.g., $M_{\rm disk}/M_{\rm S} \sim 10^{-8}$ for the B-ring (Cuzzi *et al.* 1984), where $M_{\rm disk}$ and $M_{\rm S}$ are masses of a disk and a central planet), in contrast with the case of a relatively more massive proto-lunar disk ($M_{\rm disk}/M_{\rm S} \sim 0.01$) considered in Takeda and Ida (2001). For such a less massive disk, the local approximation is valid and the local simulations enable us to examine the property of the viscosity (e.g., $\Sigma$-dependence of the viscosity) more easily.

In Section 2, we explain the procedure of the local $N$-body simulation. In Section 3, we introduce the calculation method of the viscosity, which is based on Takeda and Ida (2001). In Section 4, we show numerical results. The results show that when the wake structure is developed by the gravitational instability, angular momentum transport is significantly enhanced not only by gravitational torque due to the wake-like structure but also by the associated coherent motion of the wakes. We derive the expression of the effective viscosity in rings with wakes. In Section 5, we summarize the results and discuss the formation of the ringlet structure with radial scale $\sim$100 km in the Saturn's main ring with the obtained viscosity. The viscosity enhanced by the wakes requires more massive embedded satellites than estimated before, if these are assumed to be responsible for the gap formation in the rings.

## 2. SIMULATION METHOD AND PARAMETERS

The simulation method used in the present study is exactly the same as that used in Daisaka and Ida (1999). We consider a box with periodic boundary conditions, which is centered at the semimajor axis $a_0$ (Wisdom and Tremaine 1988). The box revolves along a circular orbit with the Kepler angular velocity $\Omega_0 = \sqrt{GM_s/a_0^3}$, where $M_s$ is the mass of a central planet. In the rotating frame, we take the local Cartesian coordinate system in which the $x$-axis points to the radial direction, the $y$-axis to the direction of motion of the box, and the $z$-axis to the direction perpendicular to the orbital plane. A particle at a position $(x,\ y,\ z)$ and with a velocity $(v_x,\ v_y,\ v_z)$ in the box has images at positions $(x + nL_x,\ y + mL_y - (3/2)nL_x\Omega_0 t,\ z)$ with velocities $(v_x,\ v_y + (3/2)nL_x\Omega_0,\ v_z)$, where $n$ and $m$ are integers, $L_x$ and $L_y$ are sizes of the box, and $t$ is the time. When a particle crosses a boundary of the original box, its image comes into the box from the opposite boundary conserving angular momentum (Wisdom and Tremaine 1988).

In the rotating, local Cartesian coordinates (see Fig. 1), particle motion is described by Hill's equation (e.g., Hill 1878, Petit and Hénon 1986, Nakazawa and Ida 1988). We hereafter consider a system of particles with identical mass $m_p$ (physical radius $r_p$) and describe it with the scaled time $\tilde{t} = t\Omega_0$ and the scaled length $\tilde{x} = x/r_p$. The normalized Hill's equations, including impulsive force $\tilde{\boldsymbol{F}}_{\rm coll}$ at an inelastic collision, are

$$\begin{cases} \ddot{\tilde{x}}_i = 2\dot{\tilde{y}}_i + 3\tilde{x}_i + \tilde{m}_p \displaystyle\sum_{j\neq i}^{N} \frac{\tilde{x}_j - \tilde{x}_i}{\tilde{r}_{ij}^3} + \tilde{F}_{{\rm coll},x}, \\ \ddot{\tilde{y}}_i = -2\dot{\tilde{x}}_i + \tilde{m}_p \displaystyle\sum_{j\neq i}^{N} \frac{\tilde{y}_j - \tilde{y}_i}{\tilde{r}_{ij}^3} + \tilde{F}_{{\rm coll},y}, \\ \ddot{\tilde{z}}_i = -\tilde{z}_i + \tilde{m}_p \displaystyle\sum_{j\neq i}^{N} \frac{\tilde{z}_j - \tilde{z}_i}{\tilde{r}_{ij}^3} + \tilde{F}_{{\rm coll},z}, \end{cases} \tag{3}$$

where $\tilde{m}_p = (4\pi a_0^3\rho/3M_s)$ and $\rho$ is the material density.

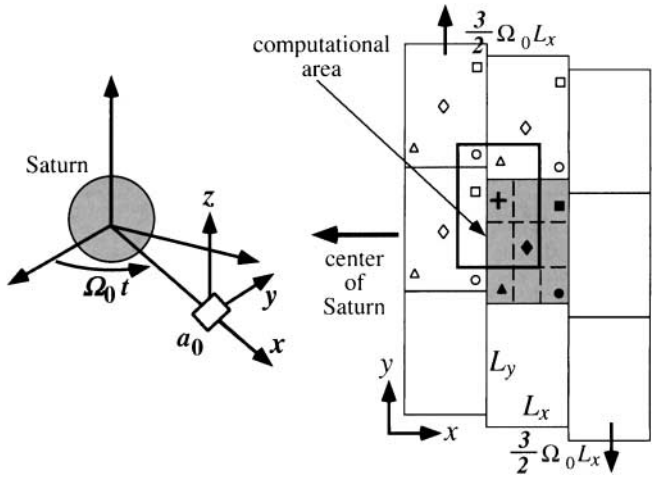


**FIG. 1.** Schematic illustrations of Hill's frame (left panel) and a computational cell (shaded area) with nine subregions (divided by broken line) for calculation of gravitational interactions between particles (right panel). Filled symbols in the computational cell denote original particles and open symbols denote their corresponding copies. The region surrounded by a thick line denotes the virtual region of a subregion, which is made for the subregion to be centered and has the same size as the computational cell. We calculated the gravitational forces exerted on particles in the subregion from particles in the virtual region, which contains copied particles.

The orbits of particles are calculated by integrating Eq. (3) with the fourth-order Hermite integrator (Makino and Aarseth 1992). A particle collision is detected as the overlapping of a colliding pair (Richardson 1994, Salo 1995, Daisaka and Ida 1999). A free-slip, hard-sphere collision model is used. Velocity after a collision (with prime symbol) is given by

$$\begin{cases} v_n' = -\varepsilon v_n, \\ v_t' = v_t, \end{cases} \tag{4}$$

where $v_n$ and $v_t$ are, respectively, the normal and tangential components of relative velocity and $\varepsilon$ is the restitution coefficient of particles in the normal direction. To avoid numerical difficulty, colliding particles are rebounded after the locations of particles are adjusted to those where they are just touching (Richardson 1994, Daisaka and Ida 1999).

We calculate gravitational forces between particles by direct sum with HARP-2 and HARP-3/GRAPE-4, which are special-purpose hardwares for calculating gravitational forces (e.g., Makino *et al.* 1993). We calculate the gravitational forces on a particle $i$ from particles in a box with $L_x$ and $L_y$, basically, centered at particle $i$ including particles in copied regions (see Fig. 1).

Next we describe the simulation parameters which characterize a particle system. The only parameters in scaled equations of motion (Eq. (3)) are the physical radius $r_p$ in $\tilde{\boldsymbol{F}}_{\rm coll}$ and the number of particle $N$ in the box and $a_0$, $M_s$, and $\rho$. It is convenient to use the non-dimensional parameters, the optical depth $\tau$ and the ratio of $r_p$ to $r_h$ instead of those parameters (Daisaka

and Ida 1999). They are defined by

$$\tau = N\pi r_{\rm p}^2/L_x L_y, \tag{5}$$

and

$$r_{\rm h}^* = \frac{r_{\rm h}}{2r_{\rm p}}, \tag{6}$$

where $r_{\rm h} = ha_0$ is the mutual Hill's radius defined as

$$r_{\rm h} = ha_0 = \left(\frac{2m_{\rm p}}{3M_{\rm s}}\right)^{1/3} a_0. \tag{7}$$

Note that $r_{\rm h}$ is the inverse of the parameter $r_{\rm p}$ used in Ohtsuki (1993) and also in Salo (1995). Measurements of the optical depth by the Voyagers gave $\tau \sim 2$ for Saturn's B-ring and $\tau \sim 0.5$ for the A-ring (e.g., Cuzzi *et al.* 1984, Esposito 1993). With the suitable parameters of Saturn's ring, $r_{\rm h}^*$ is reduced to

$$r_{\rm h}^* \simeq 0.82\left(\frac{M_{\rm s}}{5.69\times10^{26}\,{\rm kg}}\right)^{-1}\left(\frac{\rho}{900\,{\rm kg\,m^{-3}}}\right)^{1/3}\left(\frac{a_0}{10^8\,{\rm m}}\right). \tag{8}$$

The following relation between $r_{\rm h}^*$ and the Roche limit, $a_{\rm Roche} = 1.52(M_{\rm s}/\rho)^{1/3}$ (e.g., Goldreich and Tremaine 1982), is also convenient:

$$r_{\rm h}^* = 1.072\left(\frac{a_0}{a_{\rm Roche}}\right). \tag{9}$$

Within the Roche limit, Eq. (9) shows that $r_{\rm h}^* \lesssim 1$, and from Eq. (8), the parameters of Saturn's main rings also give the same relation as that for $r_{\rm h}^*$. This indicates that most of Saturn's ring is located within the Roche limit.

The physical meanings of these parameters are as follows. Equation (3) is rewritten in a dimensional form as

$$\dot{\boldsymbol{v}} = \boldsymbol{F}_{\rm c} + \boldsymbol{F}_{\rm grav} + \boldsymbol{F}_{\rm coll}, \tag{10}$$

where $\boldsymbol{F}_{\rm c}$ denotes the force from a central body (i.e., tidal and Coriolis forces), and $\boldsymbol{F}_{\rm grav}$ and $\boldsymbol{F}_{\rm coll}$ denote the self-gravity forces of particles and impulsive forces exerted on particles at collisions, respectively. Their magnitudes are

$$\begin{cases} |\boldsymbol{F}_{\rm c}| \sim v\Omega_0, \\ |\boldsymbol{F}_{\rm grav}| \sim \dfrac{v}{t_{\rm g}} \sim n\sigma_{\rm g}v^2 \sim n\pi r_{\rm h}^2 v^2, \\ |\boldsymbol{F}_{\rm coll}| \sim \dfrac{v}{t_{\rm c}} \sim n\sigma_{\rm c}v^2 \sim n\pi r_{\rm p}^2 v^2, \end{cases} \tag{11}$$

where $n$ is the number density of particles, $v$ is the typical velocity dispersion, $t_{\rm c}$ and $t_{\rm g}$ are the mean collision time and relaxation time due to self-gravitational interactions, and $\sigma_{\rm c}$ and $\sigma_{\rm g}$ represent corresponding cross sections. Relative importance of these forces corresponds to $\tau$ and $r_{\rm h}^*$ as

$$\begin{cases} \dfrac{|\boldsymbol{F}_{\rm coll}|}{|\boldsymbol{F}_{\rm c}|} \sim \dfrac{v/t_{\rm c}}{\Omega_0 v} \sim \dfrac{t_{\rm K}}{t_{\rm c}} \sim \tau, \\ \dfrac{|\boldsymbol{F}_{\rm grav}|}{|\boldsymbol{F}_{\rm coll}|} \sim \dfrac{t_{\rm c}}{t_{\rm g}} \sim r_{\rm h}^{*2}, \end{cases} \tag{12}$$

where $t_{\rm K}$ is the Keplerian time. When $\tau \gtrsim 1$ and $r_{\rm h}^* \gtrsim 0.5$, the self-gravity and effects of energy dissipation through inelastic collisions are comparable to or stronger than the tidal force. Self-gravity and energy dissipation tend to lead a system to an unstable state, so it leads to the formation of non-uniform structure such as wakes and particle aggregates, while the tidal force tends to smooth out the non-uniform structure. An apparent non-uniform structure is formed when $\tau \gtrsim 1$ and $r_{\rm h}^* \gtrsim 0.5$ (Salo 1995, Daisaka and Ida 1999).

Ohtsuki and Emori (2000) gave the criterion of the wake formation more quantitatively by using the Toomre's $\mathcal{Q}$ parameter. The definition of the $\mathcal{Q}$ value (see Eq. (1)) shows that the condition for the self-gravitational instability depends on the velocity dispersion of particles as well as the surface density in the particle system. According to the local $N$-body simulations (Salo 1995, Daisaka and Ida 1999) and the analytic and three-body calculations (Ohtsuki 1999), if $r_{\rm h}^* \gtrsim 0.5$, the velocity dispersion is regulated to be surface escape velocity, $\sigma_r \simeq \sqrt{Gm_{\rm p}/r_{\rm p}}$, whereas if $r_{\rm h}^* \lesssim 0.5$, it is regulated by collisions to be $\sigma_r \sim 2r_{\rm p}\Omega_0$. Therefore, the condition for the wake formation, $\mathcal{Q} \lesssim 2$, is

$$\tau \gtrsim \begin{cases} 0.08 r_{\rm h}^{*-3} & \text{for } r_{\rm h}^* \lesssim 0.5 \text{ (i)}, \\ 0.2 r_{\rm h}^{*-3/2} & \text{for } r_{\rm h}^* \gtrsim 0.5 \text{ (ii)}. \end{cases} \tag{13}$$

Furthermore, particle aggregates are formed against tidal effect for $r_{\rm h}^* \lesssim 1$; the stringent condition is $r_{\rm h}^* \gtrsim 3/2$, and $1 \lesssim r_{\rm h}^* \lesssim 3/2$ is the intermediate range, where accretion may be possible but is quite difficult (Ohtsuki 1993, Salo 1995).

The above conditions are consistent with our numerical results. We plot in Fig. 2 these conditions by thin (condition (i)) and thick (condition (ii)) solid lines as well as spatial distributions of particles obtained from our simulations with various values of $\tau$ and $r_{\rm h}^*$ ($\varepsilon = 0.4$ in cases of $r_{\rm h}^* = 0.675$ and 0.5 otherwise). Our results show the wake formation in the region where Eq. (13) is satisfied. Salo (1995) also discussed the condition of wake formation, comparing velocity dispersions due to collisions and self-gravitational encounters between particles with those due to collective effects of wakes. The suggestion of Salo (1995) for this condition is that velocity dispersion due to wakes becomes larger than that due to collisions and gravitational scatterings, and it was confirmed by his simulations. This condition is essentially the same as Eq. (13), since in Salo (1995) velocity dispersion due to wakes is supposed to be expressed by $\mathcal{Q} \simeq 2$.

Observed parameters of Saturn's main ring correspond to $\tau \gtrsim 0.5$ and $r_{\rm h}^* \gtrsim 0.5$ (e.g., Esposito 1993). Figure 2 indicates that wake structure could develop in Saturn's main ring. The presence of such a small-scale, wake-like structure obtained from

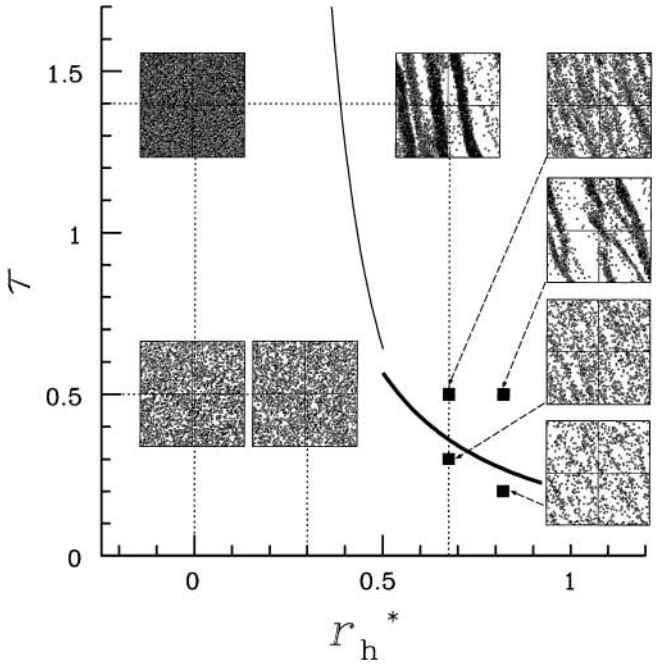


**FIG. 2.** Spatial distribution obtained from simulations with various values of optical depth $\tau$ and $r_h^*$. In a series of simulations with fixed $r_h^* = 0.675$, we assumed the normal restitution coefficient to be $\varepsilon = 0.4$. In the other simulations, $\varepsilon = 0.5$. All panels are trimmed to have the same size with width $L = 125$ m and we assumed particle radius $r_p = 1$ m. Except for simulations with $r_h^* = 0$, we used a larger size of a computational cell than displayed here. Thin and thick lines present conditions (i) and (ii), which are the conditions for the gravitational instability (see Eq. (13)).

the local $N$-body simulations may be supported by observations of asymmetrical features in Saturn's A-ring (e.g., Franklin *et al.* 1987, Dones *et al.* 1993, van der Tak *et al.* 1999) and PPS observation of hyperfine structures ($\sim$100-m scale structures) by Voyager (e.g., Esposito 1993). Thus, to estimate the viscosity in the main ring, we have to include the effects of the wakes.

It should be noted that the restitution coefficient is also a simulation parameter to regulate the strength of $\boldsymbol{F}_{\rm coll}$. The inelasticity of a ring particle depends on impact velocity as well as its material property (e.g., Bridges *et al.* 1984), but it is not yet to be understood well. However, in the case where the wakes strongly develop, physical (dynamical) properties of the system seem independent of, or only weakly dependent on the inelasticity, as shown later. Hence, we mainly concentrate on the two parameters $\tau$ and $r_h^*$ in the present study.

## 3. FORMULATION OF ANGULAR MOMENTUM TRANSPORT AND RING'S VISCOSITY

According to Wisdom and Tremaine (1988) and Takeda and Ida (2001), we describe the formulation of the angular momentum flux and the viscosity in a dense ring system where both self-gravity and physical collision are important.

As described in Section 1, the angular momentum transport is divided into the following three components:

1. translational (local, streaming) transport, which is caused by the particle transport,
2. collisional transport, which is originated from the nonlocal effect of collisions,
3. gravitational transport, which is due to the self-gravitational torque.

From these components of the angular momentum flux, we obtain the corresponding viscosity, as shown below. To avoid confusion, we list in Table I symbols for the viscosity used in the present study and previous works.

Let us consider the rate of change in angular momentum in an annular region with surface density $\Sigma$ at radius $r$. Takeda and Ida (2001) derived the angular momentum change rate in the annular region based on the Boltzmann equation as

$$\frac{\partial}{\partial t}(2\pi r\,\Sigma(r) r U_\theta(r)) = -\frac{\partial}{\partial r}(\Phi_{\rm trans} + \Phi_{\rm coll} + \Phi_{\rm grav}), \quad (14)$$

where $U_\theta(r)$ is the mean tangential velocity averaged over $\theta$ and $\Phi_{\rm trans}$, $\Phi_{\rm coll}$, and $\Phi_{\rm grav}$ are the angular momentum fluxes due to the translational, collisional, and gravitational transports, respectively. Note that, in Eq. (14), the advective term, which expresses angular momentum flux due to mean radial flow and appears in Takeda and Ida (2001), vanishes because we assume that the radial velocity averaged over $\theta$ is zero. Each component of the angular momentum flux is expressed by the distribution function $f(\boldsymbol{x}, \boldsymbol{v}, t)$ in phase space as

$$\begin{cases} \Phi_{\rm trans} \equiv r^2 \displaystyle\int_0^{2\pi} d\theta \int_{-\infty}^{\infty} dz \int d\boldsymbol{v}\; v_r\; v_\theta\; f(\boldsymbol{x}, \boldsymbol{v}, t) m, \\ \Phi_{\rm coll} \equiv -\displaystyle\int_{r_{\rm min}}^{r} dr' \int_0^{2\pi} d\theta \int_{-\infty}^{\infty} dz \left[\frac{\partial}{\partial t} r'^2 \rho u_\theta(\boldsymbol{r})\right]_c, \\ \Phi_{\rm grav} \equiv \displaystyle\int_{r_{\rm min}}^{r} dr' \int_0^{2\pi} d\theta' \int_{-\infty}^{\infty} dz'\, r'\, \rho(\boldsymbol{r}') \frac{\partial \varphi_{\rm self}}{\partial \theta'}(\boldsymbol{r}'), \end{cases} \quad (15)$$

**TABLE I**
**Symbols Describing the Viscosity Used in Previous and Present Studies**

| Component | Goldreich and Tremaine (1978a) | Araki and Tremaine (1986) | Wisdom and Tremaine (1988) | In this work |
|---|---|---|---|---|
| 1. Local (or stream, translational) | $\nu$ | | $\nu_{\rm L}$ | $\nu_{\rm trans}$ $\frac{\nu_{\rm trans,local}}{\nu_{\rm trans,bulk}}$ |
| 2. Non-local (or collisional) | — | | $\nu_{\rm NL}$ | $\nu_{\rm coll}$ |
| 3. Gravitational | — | | — | $\nu_{\rm grav}$ |

*Note.* In Araki and Tremaine (1986) and Wisdom and Tremaine (1988), subscripts N and NL denote local and non-local, respectively. Later, $\nu_{\rm trans}$ is split into two components of $\nu_{\rm trans,local}$ and $\nu_{\rm trans,bulk}$, which come from local random motion and systematic bulk motion of particles, respectively (see Section 5).

where $\varphi_{\rm self}$ is the gravitational potential defined as

$$\varphi_{\rm self} = -G \int \frac{\rho(\boldsymbol{r}')}{|\boldsymbol{r} - \boldsymbol{r}'|}\, d^3\boldsymbol{r}', \tag{16}$$

and $m$ is the particle mass, $r_{\rm min}$ is the inner boundary of the ring. With the distribution function $f(\boldsymbol{x}, \boldsymbol{v}, t)$, the density $\rho$ and the mean velocity $u_i$ are given by

$$\begin{cases} \rho(r) = \int m f(\boldsymbol{x}, \boldsymbol{v}, t)\, d\boldsymbol{v}, \\ \rho u_i(r) = \int m f(\boldsymbol{x}, \boldsymbol{v}, t)\, v_i\, d\boldsymbol{v}. \end{cases} \tag{17}$$

In a Keplerian disk, the (total) angular momentum flux $\Phi_{\rm vis}$ is related to the kinematic viscosity $\nu$ as (Lynden-Bell and Pringle 1974)

$$\Phi_{\rm vis} = 3\pi \Sigma \nu \Omega_0 r^2. \tag{18}$$

Since the total flux consists of three components (Eq. (15)), we also introduce three corresponding components of the viscosity: the transrational, collisional, and gravitational viscosity, which are related to the components of the flux in the same way as Eq. (18). The total viscosity is given by the sum of these components. By substituting $f(\boldsymbol{x}, \boldsymbol{v}, t) = \Sigma_i \delta(\boldsymbol{x}_i - \boldsymbol{x})\delta(\boldsymbol{v}_i - \boldsymbol{v})$, where $\delta$ is the Dirac's $\delta$-function, into Eqs. (15) and (18), these components of the viscosity in the Hill's frame are given by

$$\begin{cases} \nu_{\rm trans} = \dfrac{2}{3\Omega_0 \sum_i m_i} \sum_i m_i \dot{x}_i \dot{y}_{r,i}, \\ \nu_{\rm coll} = \dfrac{2}{3\Omega_0 \sum_i m_i} \dfrac{1}{\Delta T} \sum_{\rm coll} \Delta p_{y>} (x_> - x_<), \\ \nu_{\rm grav} = \dfrac{2}{3\Omega_0 \sum_i m_i} (-G) \sum_i \sum_{j\, x_j > x_i} m_i m_j \dfrac{(y_j - y_i)(x_j - x_i)}{|x_j - x_i|^3}, \end{cases} \tag{19}$$

where $\dot{y}_{r,i} = \dot{y}_i + (3/2)\Omega_0 x_i$ is the $y$-component of the relative velocity to the mean shear velocity at $x_i$, subscripts $<$ and $>$ mean particles inside and outside at a collision and $\Delta p_{y>}$ is the $y$-component of momentum change by the collision. The summation in $\nu_{\rm coll}$ is done for all collisions during the time interval $\Delta T$. The summation of $i$ in $\nu_{\rm grav}$ is done for all particles in the original box and that of $j$ is done for all particles with $x_j > x_i$ in the original and image boxes. The derivation of $\nu_{\rm grav}$ is given in the Appendix and the expressions of $\nu_{\rm trans}$ and $\nu_{\rm coll}$ are the same as those in Wisdom and Tremaine (1988), in which they were called local and non-local components, respectively. These viscosities are evaluated from the results of our simulations by taking the time average after a system establishes a quasi-equilibrium state, because when wakes strongly develop, the viscosities fluctuate with large magnitude.

In previous studies on accretion disks, as mentioned in the Introduction, influences of the gravitational instability on angular momentum transport was examined, but only the total angular momentum flux was evaluated macroscopically (Anthony and Carlberg 1988, Laughlin and Bodenheimer 1994, Laughlin and Rozyczka 1996). In contrast, we numerically evaluate ring viscosity from the microscopic viewpoint as in Eq. (19).

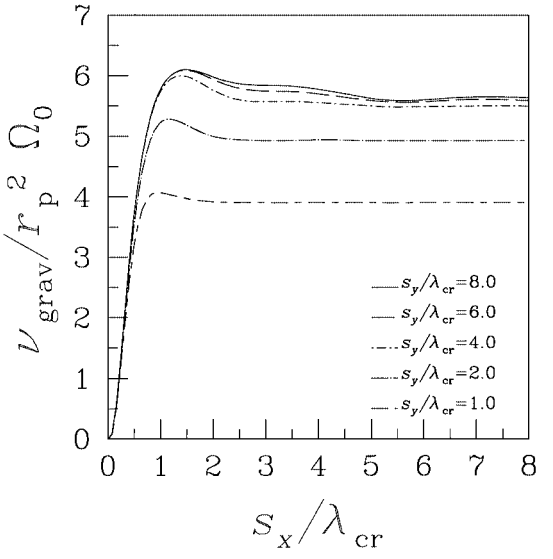


**FIG. 3.** $\nu_{\rm grav}$ as a function of $s_x$ scaled by $\lambda_{\rm cr}$ with fixed $s_y/\lambda_{\rm cr} = 1.0$ (short dashed–long dashed line), 2.0 (dotted–long dashed line), 4.0 (dotted–short dashed line), 6.0 (dashed line), and 8.0 (solid line). Simulation parameters used here are $\tau = 0.5$, $r_{\rm h}^* = 0.82$, and $\varepsilon = 0.5$. The size of a simulation cell and number of particles are $L_x = L_y = 12\lambda_{\rm cr}$ and $N = 39788$.

In principle, the summation for $\nu_{\rm grav}$ in Eq. (19) should be done for all existing particles, but in practice we need a cut-off of self-gravity. We examine the influence of the cut-off of self-gravity on the gravitational torque, calculating $\nu_{\rm grav}$ in Eq. (19) with cut-off distance. We set the cut-off distance of an $i$-particle as $|x_j - x_i| < s_x/2$ and $|y_j - y_i| < s_y/2$, where $s_x$ and $s_y$ are the width and height of a cell centered on the $i$-particle. In Fig. 3, we plot $\nu_{\rm grav}$ as a function of $s_x$ with fixed $s_y$ obtained from the simulation for $\tau = 0.5, r_{\rm h}^* = 0.82, \varepsilon = 0.5$ with larger computational area ($L_x = L_y = 12\lambda_{\rm cr}$, where $\lambda_{\rm cr}$ is the critical wavelength and the number of particles $N = 39788$), which shows the apparent wake structure (see Fig. 2). Note that the summation of $j$ is also done with $x_j > x_i$. Figure 3 shows that as both $s_x$ and $s_y$ take larger values, $\nu_{\rm grav}$ tends to converge on a certain value, which depends on the parameters used in the simulation. In order to obtain $\nu_{\rm grav}$ with enough accuracy, we need $s_x$ and $s_y$ to be larger than $3$–$4\lambda_{\rm cr}$. Also, this value corresponds to the size of a simulation cell required for simulations with the wakes. A similar result is obtained from simulations with different parameters which also lead to wake formation. In this study, we use a cell size larger than $3\lambda_{\rm cr} \times 3\lambda_{\rm cr}$.

## 4. NUMERICAL RESULTS

In order to evaluate the viscosity (or the angular momentum flux) in planetary rings, we performed the following six series

of simulations: (i) simulations with various values of the optical depth $\tau$ for fixed $r_h^* = 0$ and $\varepsilon = 0.5$, (ii) those for fixed $r_h^* = 0.675$ and $\varepsilon = 0.4$, (iii) those for fixed $r_h^* = 0.7$ and $\varepsilon = 0.1$, (iv) simulations with various values of the ratio $r_h^*$ for fixed $\tau = 0.2$ and $\varepsilon = 0.5$, (v) those for $\tau = 0.5$, and (vi) those for $\tau = 1.0$ and $\varepsilon = 0.1$. Note that set (i) corresponds to a non-self-gravitating case. The details of sizes of the computational area and the number of particles used in simulations are listed in Tables II and III.

First we show the results of set (i) (the non-self-gravity case) to check the validity of our numerical results. This set has the same parameters as set (2) in Wisdom and Tremaine (1988), except that we use a computational area much larger than that used in Wisdom and Tremaine (1988) (we use $L = 125 r_p$ with $N \gtrsim 500$ particles; for example, $N = 498$ for $\tau = 0.1$ and $N = 9948$ for $\tau = 2.0$, but Wisdom and Tremaine (1988) used $L \lesssim 25 r_p$ with constant $N = 40$). The normalized viscosity $[\nu/(r_p^2 \Omega_0/\tau)]$ obtained from our simulations as well as the results of Wisdom and Tremaine (1988) is plotted in Fig. 4. They show good agreement.

In Fig. 4, numerical results show that in an optically thin region ($\tau < 0.6$), $\nu_{trans}$ is larger than $\nu_{coll}$ whereas in an optically thick case ($\tau > 0.6$), $\nu_{coll}$ is the dominant component in the viscosity. Such a property is explained by the results of the analytical studies by Goldreich and Tremaine (1978a) and Araki and Tremaine (1986). In Fig. 4, we also plotted their analytical results,

$$\nu_{trans} \simeq \frac{\sigma_r^2}{2\Omega_0}\left(\frac{0.46\tau}{1+\tau^2}\right), \tag{19}$$

and

$$\nu_{coll} \sim r_p^2 \Omega_0 \tau, \tag{20}$$

**TABLE II**

**Number of Particles and Size of Computational Area Used in Simulations with Various Values of Optical Depth $\tau$ for $r_h^*$ = 0, 0.675, and 0.7**

| | Set (i) [$r_h^* = 0$] | Set (ii) [$r_h^* = 0.675$] | | | Set (iii) [$r_h^* = 0.7$] | |
|---|---|---|---|---|---|---|
| $\tau$ | $N$ | $N$ | $L_x/\lambda_{cr}$ | $L_y/\lambda_{cr}$ | $N$ | $L_x/\lambda_{cr}$ |
| 0.01 | 198 | 198 | 539.06 | 539.06 | 198 | 483.34 |
| 0.05 | 994 | 994 | 108.81 | 108.81 | 994 | 96.67 |
| 0.1 | 498 | 5059 | 86.18 | 86.18 | 1990 | 48.33 |
| 0.2 | 994 | 4992 | 30.21 | 30.21 | 3978 | 24.16 |
| 0.3 | 1492 | 5052 | 16.53 | 16.53 | — | — |
| 0.4 | 1990 | 5092 | 10.79 | 10.79 | — | — |
| 0.5 | 2486 | 5156 | 7.77 | 7.77 | — | — |
| 0.6 | 2984 | 4890 | 5.75 | 5.75 | — | — |
| 0.7 | 3482 | 5014 | 4.62 | 4.62 | — | — |
| 0.8 | 3978 | 4992 | 3.74 | 3.74 | — | — |
| 0.9 | 4476 | 4842 | 3.12 | 3.12 | — | — |
| 1.0 | 4974 | 9200 | 3.67 | 3.67 | 30656 | 6.0 |
| 1.2 | 5968 | 42780 | 5.75 | 6.29 | — | — |
| 1.4 | 6964 | 17826 | 3.08 | 3.08 | — | — |
| 1.6 | 7958 | — | — | — | — | — |
| 1.8 | 8952 | — | — | — | — | — |
| 2.0 | 9948 | — | — | — | — | — |

*Note.* Size of computational area is scaled by the critical wavelength $\lambda_{cr}$ for each parameter. Restitution coefficient is $\varepsilon = 0.4$ and 0.5 for set (i), $\varepsilon = 0.4$ for set (ii), and $\varepsilon = 0.1$ for set (iii). In non-gravitating cases ($r_h^* = 0$), size of computational area is $L = 125 r_p$ except for the cases of $\tau = 0.01$ and 0.05, in which the size is $L = 250 r_p$. A square region was used for all simulations in sets (i) and (iii).

**TABLE III**

**Number of Particles and Size of Computational Area Used in Simulations with Various Values of $r_h^*$ for Fixed $\tau$ = 0.2, 0.5, and 1.0**

| | Set (iv) [$\tau = 0.2$] | | Set (v) [$\tau = 0.5$] | | | Set (vi) [$\tau = 1.0$] | |
|---|---|---|---|---|---|---|---|
| $r_h^*$ | $N$ | $L_x/\lambda_{cr}$ | $N$ | $L_x/\lambda_{cr}$ | $L_y/\lambda_{cr}$ | $N$ | $L_x/\lambda_{cr}$ |
| 0.3 | 2062 | 220.6 | 5156 | 88.50 | 88.50 | — | — |
| 0.5 | 2062 | 47.7 | 5156 | 19.10 | 19.10 | 4072 | 6.0 |
| 0.6 | 2062 | 27.6 | 5156 | 11.05 | 11.05 | 12158 | 6.0 |
| 0.65 | 2026 | 21.7 | 5156 | 8.69 | 8.69 | 19652 | 6.0 |
| 0.675 | 2026 | 19.4 | 5458 | 8.0 | 8.0 | — | — |
| 0.7 | 2062 | 17.40 | 5156 | 6.97 | 6.97 | 30658 | 6.0 |
| 0.75 | 2026 | 14.1 | 3184 | 3.14 | 6.28 | — | — |
| 0.8 | 2062 | 11.66 | 8566 | 6.01 | 6.01 | 68308 | 6.0 |
| 0.82 | — | — | 9948 | 6.01 | 6.01 | — | — |
| 0.85 | 2062 | 9.7 | 6238 | 3.02 | 6.04 | — | — |
| 0.9 | 2062 | 8.19 | 17332 | 6.00 | 6.00 | — | — |
| 0.95 | 2062 | 7.0 | 12104 | 3.02 | 6.04 | — | — |
| 1.00 | 2062 | 6.0 | 16838 | 3.05 | 6.10 | — | — |

*Note.* Size of computational area is scaled by $\lambda_{cr}$ for each parameter and square region was used for all simulations for sets (iv) and (vi). Restitution coefficient is $\varepsilon = 0.5$ for sets (iv) and (v), $\varepsilon = 0.1$ for set (vi).

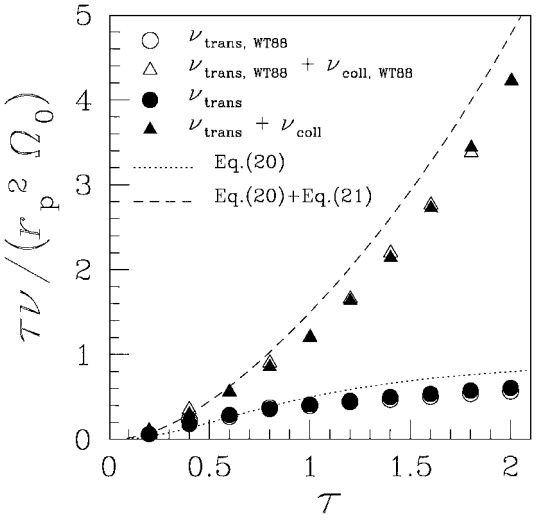


**FIG. 4.** Comparison of set (i) with Wisdom and Tremaine (1988) and the analytical estimations without self-gravity. Circles and triangles denote $\nu_{trans}$ and $\nu_{trans} + \nu_{coll}$. Open and filled symbols are our results and those of Wisdom and Tremaine (1988). Dotted and broken lines represent analytical results given by Eq. (20) and the sum of Eqs. (20) and (21).

where $\sigma_r$ is the random velocity of particles, which could be estimated as $\sigma_r \sim 2r_p\Omega_0$. These analytical formulas are consistent with the numerical results.

Now, we show the results in self-gravitating cases. In Fig. 5, we plot the total viscosity as a function of $r_h^*$ for sets (iv)–(vi). As shown in Fig. 5, for all $\tau$, the total viscosity is almost constant for $r_h^* < 0.5$. The constant value agrees with that obtained from the non-self-gravitating simulations. For $r_h^* > 0.5$, the viscosity increases rapidly with $r_h^*$, in accordance with the region where Hill's radius of particles is greater than their physical radius and the self-gravity plays important roles in dynamical properties of particles. Figure 6 shows the total viscosity as a function of $\tau$ for sets (i)–(iii). A comparison between sets (i) and (ii) clearly shows that the self-gravity increases the viscosity for all $\tau$. For the parameters of Saturn's B-ring ($r_h^* \simeq 0.8$), the enhancement factor is greater than 10 in large $\tau$ cases ($\tau = 0.5$ and 1.0) and greater than 2 even in the case of $\tau = 0.2$. The strong enhancement for large $\tau$ is related to the wake structure, as will be shown below.

Petit and Hénon (1987a, 1987b, 1988) have investigated evolution of planetary rings, taking into account both self-gravitational forces and inelastic collisions between particles. They derived a formula for mass flux in a ring, by calculating the cumulative effect of individual pairwise encounters due to the self-gravity and collision. Their calculation would be valid for optically thin rings ($\tau \ll 1$), where mean free time is, at most, a Keplerian time. Their formula for the mass flux gives the viscosity in an optically thin ring since the mass diffusion is related to the viscosity. Petit and Hénon presented the mass flux $\Phi_M$ in a non-dimensional form (see Eq. (18) of Petit and Hénon 1988).

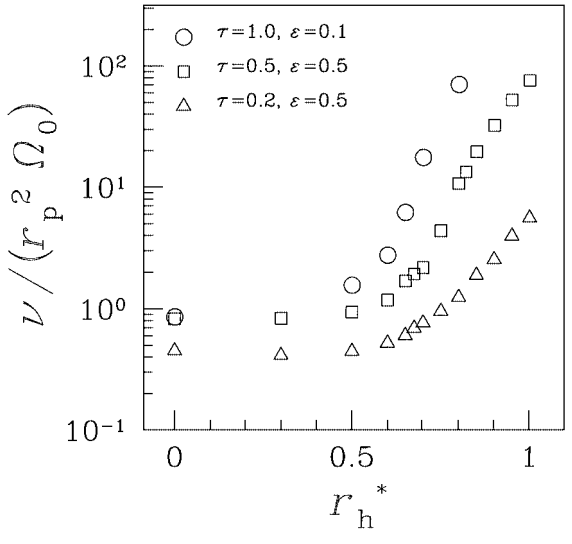


**FIG. 5.** Ring's total viscosity as a function of $r_h^*$ for set (iv) [$\tau = 0.2$, triangles], set (v) [$\tau = 0.5$, squares], and set (vi) [$\tau = 1.0$, circles]. Note that in the non-self-gravitating case ($r_h^* = 0$), the viscosity for $\tau = 1.0$ is somewhat smaller than that for $\tau = 0.5$ because of the difference of restitution coefficient used in the simulations.

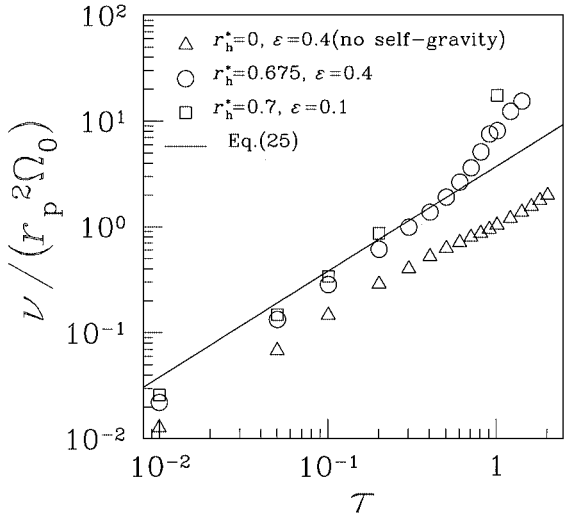


**FIG. 6.** Ring's total viscosity as a function of optical depth $\tau$ for set (i) [$r_h^* = 0$, triangles], set (ii) [$r_h^* = 0.675$, circles], and set (iii) [$r_h^* = 0.7$, squares]. Normal restitution coefficient is $\varepsilon = 0.4$ for set (i) and set (ii), $\varepsilon = 0.1$ for set (iii). The solid line represents the viscosity estimated by using mass flux formula obtained by Petit and Hénon (1988).

Their formula is rewritten in a dimensional form as

$$\Phi_M = -\frac{3}{4}\pi I \left(\frac{2m_p}{M_s}\right)^{4/3} \frac{a_0^5}{m_p}\frac{\partial \Sigma^2}{\partial a}\Omega_0, \tag{21}$$

where $\Sigma$ and $m_p$ represent the surface density and the mass of a ring particle, respectively, and $I$ is a non-dimensional factor, which depends on $r_h^*$ and $\varepsilon$. In the formula, it is assumed that $|\partial\Sigma/\partial a| \gg \Sigma/a$ since a local coordinate system is used in their derivation. The quantities with the subscript 0 mean those at the local coordinate system. In the above, we assumed an equal-mass particle system though they also examined a system with mass distribution of particles. Note that, instead of $\Sigma$, they used the non-dimensional surface density $g$ given by $m_p g = 2\pi a_0^2 \Sigma (2m_p/M_s)^{1/3}$. On the other hand, in a Keplerian viscous disk, the mass flux is given by (Lynden-Bell and Pringle 1974)

$$\Phi_M = -6\pi a^{1/2}\frac{d}{da}(a^{1/2}\nu\Sigma). \tag{22}$$

Comparing Eq. (22) with Eq. (23) and using the above local approximation for $\Sigma$, we obtain the viscosity in optically thin rings as[2]

$$\nu = \frac{1}{8} I \left(\frac{2m_p}{M_s}\right)^{4/3} a_0^4 \Omega_0 \frac{\Sigma}{m_p}, \tag{23}$$

[2] A similar relation was obtained by Petit and Hénon (1988), but their relation is different from Eq. (24) by factor 2. This is because they assumed that the viscosity is independent of $a$ but it depends on $a$ as well as $\Sigma$.

where we assumed that the viscosity vanishes in the limit of $\Sigma \to 0$. Equation (24) shows that $\nu \propto \Sigma$. It is also expressed with the parameters $\tau$ and $r_h^*$ as

$$\nu = 2.75 I r_h^{*4} \tau r_p^2 \Omega_0, \tag{24}$$

where we used Eq. (6) and the relation that $\Sigma = m_p \tau/(\pi r_p^2)$ obtained from Eq. (5). As to the factor $I$, Petit and Hénon (1987a) obtained $I = 5.78$ for $r_h^* = 0.70$ and $\varepsilon = 0.1$.

In Fig. 6, we also plotted the viscosity calculated from Eq. (25). The factor $I$ is assumed to be 5.78. The comparison of our results with Eq. (25) makes the effect of the wake structure on the viscosity rather clear, since Petit and Hénon assumed independent pairwise encounters. For example, the viscosity in the case with $\tau = 1.0$, $r_h^* = 0.7$, and $\varepsilon = 0.1$, which exhibits the wake formation, is considerably larger than the value expected by Eq. (25). In set (ii) ($r_h^* = 0.675$, $\varepsilon = 0.4$), enhancement of the viscosity occurs for $\tau > 0.6$. On the other hand, Fig. 6 shows that in the simulations with low optical depth, the viscosity almost agrees with Eq. (25). However, even in small $\tau$ region, the viscosity of our results for $r_h^* = 0.7$, $\varepsilon = 0.1$ is somewhat smaller than Eq. (25). For example, the difference is about 30% for $\tau = 0.01$. The calculation by Petit and Hénon is a two-dimensional calculation; that is, particles are assumed to distribute in the mid-plane. The self-gravity of such a 2D ring is larger than that of a 3D ring, which would account for the above difference.

In Fig. 7, the total viscosity shown in Figs. 5 and 6 is split into the translational, collisional, and gravitational components. Figure 7a shows the results in set (v) (we plotted the viscosity only in the region $r_h^* \geq 0.5$). In Fig. 7b, the results in set (ii) are shown with the results of the non-self-gravitating case (set (i) but $\varepsilon = 0.4$). For $r_h^* \gtrsim 0.7$ and $\tau \gtrsim 0.5$, wakes appear (Fig. 2). In such a parameter region, the translational and gravitational viscosity are similar to each other. Figure 7a shows that for large $r_h^*$ region ($r_h^* > 0.7$), the above two components dominate the collisional component. For small $r_h^*$ region ($r_h^* \leq 0.6$), where the wake structure does not emerge, the gravitational viscosity is much smaller than the other components.

Figure 7b shows that the translational viscosity is enhanced in large $\tau$ region. This enhancement is caused by coherent motion of particles in the wakes due to the self-gravity, as shown in the next section. Richardson (1994) evaluated $\nu_{\rm trans}$ and $\nu_{\rm coll}$ from the results of his local $N$-body simulations but did not find the enhancement of the translational viscosity. This would be because his computational area was not large enough compared with the scale of the wakes. The formation of the wakes is essential to the enhancement of the viscosity.

We also show the dependence of the viscosity on the normal restitution coefficient $\varepsilon$. In Fig. 8, the results with various values of the velocity-independent restitution coefficient $\varepsilon$ for fixed parameters $\tau = 0.5$ and $r_h^* = 0.675$ are shown. The size of the computational area and number of particles used in the simulations are $L/\lambda_{\rm cr} = 8.0$ and $N = 5458$. In this case, we found the wake formation for $\varepsilon \lesssim 0.4$. In such a region, results are almost independent of $\varepsilon$: $\nu_{\rm trans}$ and $\nu_{\rm grav}$, take a similar value independent of $\varepsilon$, and are dominant in the viscosity. On the other hand, in a large $\varepsilon$ region ($\varepsilon \gtrsim 0.5$), no wake structure is observed because less collisional damping results in so large an equilibrium velocity as to avoid the gravitational instability. Also such a large equilibrium velocity results in a large amount of $\nu_{\rm trans}$ and it varies with $\varepsilon$, as shown in Fig. 8. Since the tangential component of the restitution coefficient $\varepsilon_t = 1$ in our simulations, the case of $\varepsilon \gtrsim 0.5$ means that the effective restitution coefficient given by $\varepsilon_{\rm eff} \simeq \sqrt{(\varepsilon_t^2 v_t^2 + \varepsilon^2 v_n^2)/(v_t^2 + v_n^2)}$ (Canup and Esposito 1995) is $\gtrsim 0.8$, where the averaged tangential and normal collision

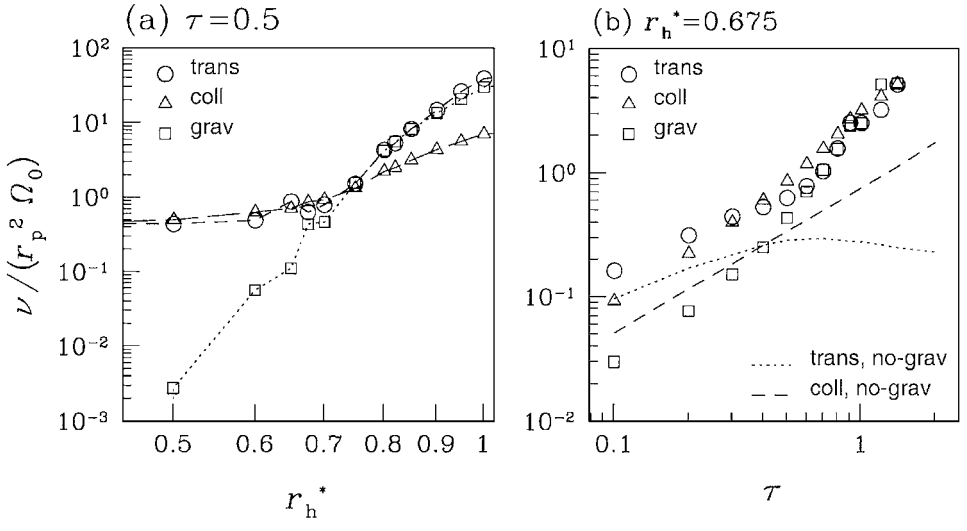


**FIG. 7.** Separation of the total viscosity in Figs. 5 and 6 into individual components for (a) set (v) and (b) set (ii). Circles, triangles, and squares denote the translational, collisional, and gravitational viscosity, respectively. We also draw the translational and collisional viscosity without self-gravity (set (i) except for $\varepsilon = 0.4$) by dotted and broken lines, respectively.

velocities are assumed to be the same. Except for such highly elastic cases, the features of the viscosity depend on $\varepsilon$ only weakly.

In addition, we briefly discuss the case of velocity-dependent restitution coefficient $\varepsilon(v)$. Salo (1995) has studied the influence of the inelastic property on the wake formation by performing simulations with two different functional forms of restitution coefficient; one is given by Bridges *et al*. (1984) and the other is the Dilley-type model (Dilley 1993). The Dilley-type model is a proposed theoretical model fitting the experimental results of Hatzes *et al*. (1988) and is generally a less dissipative model than the Bridges-type model. Salo (1995) showed that, in simulations for $\tau = 0.4$, the Dilley-type model does not lead to the wake formation because the equilibrium velocity dispersion is large enough to suppress the gravitational instability in such small $\tau$ case, while for the Bridges-type model it is possible to give a qualitatively similar behavior as in the constant $\varepsilon$ cases and show the wakes. However, even for the Dilley-type model, the wake formation should take place if $\tau$ is large enough. According to Salo (1995), the equilibrium velocity in the Dilley-type model without self-gravity may range for $10 \sim 40 r_p \Omega_0$, which is much larger than the value estimated in the velocity-independent, restitution coefficient case ($\sim r_p \Omega_0$). For a such large velocity dispersion, the condition for the wake formation, $Q \lesssim 2$, requires large $\tau$ as $0.7 \lesssim \tau \lesssim 2.8$. Hence, the inelastic property also plays important roles on the condition for the wake formation. On the other hand, in the presence of strongly developed wakes, the restitution coefficient $\varepsilon(v)$ would affect the viscosity insignificantly, as seen in the constant $\varepsilon$ cases. This is verified in the additional simulation with the Bridges-type restitution coefficient for $\tau = 1.0$ and $r_h^* = 0.82$, which produces results of the viscosity quantitatively similar to the simulation with $\varepsilon = 0.5$, as shown in Table IV.

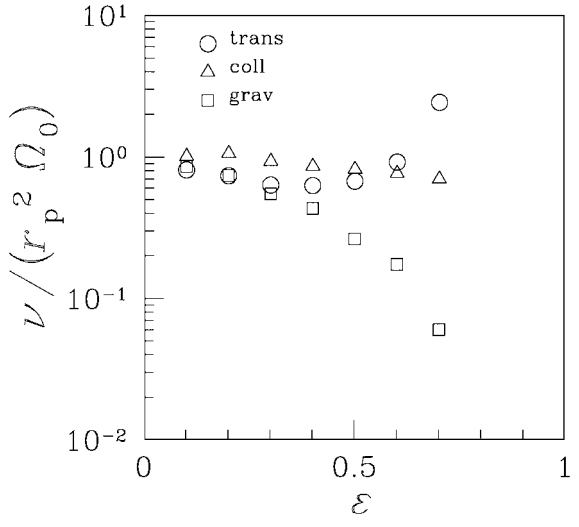


**FIG. 8.** Components of the viscosity as a function of restitution coefficient $\varepsilon$. Simulation parameters are $\tau = 0.5$ and $r_h^* = 0.675$. For $\varepsilon > 0.7$, there is no steady state, in agreement with the results of Goldreich and Tremaine (1978a) and Ohtsuki (1999).

**TABLE IV**
**Comparison of the Viscosity Obtained from Simulations with the Bridges-Type Model and Fixed Restitution Coefficient $\varepsilon$ = 0.5**

| | $\nu_{\rm trans}$ | $\nu_{\rm coll}$ | $\nu_{\rm grav}$ |
|---|---|---|---|
| Bridges-type | $3.791 \times 10$ | $1.551 \times 10$ | $4.295 \times 10$ |
| $\varepsilon = 0.5$ | $2.911 \times 10$ | $1.354 \times 10$ | $3.547 \times 10$ |

*Note*. In both simulations, we set $\tau = 0.1$, $r_h^* = 0.82$, and size of a simulation cell to be $6\lambda_{\rm cr} \times 6\lambda_{\rm cr}$, which needs a number of particles $N = 79578$. Note that the viscosity is scaled by $r_p^2 \Omega_0$.

## 5. DETAILED ANALYSIS OF THE TRANSLATIONAL AND GRAVITATIONAL VISCOSITY

As seen in the numerical results, when wakes are induced by the self-gravity, the component of $\nu_{\rm grav}$ has a large contribution to the viscosity and $\nu_{\rm trans}$ is considerably enhanced compared with that in the non-self-gravitating case. Also $\nu_{\rm coll}$ is enhanced compared with non-self-gravitating cases due to increases in the number of collisions in the wakes, but its relative importance is reduced as increasing $r_h^*$. Then, we found that $\nu_{\rm trans} \sim \nu_{\rm grav} \gtrsim \nu_{\rm coll}$. In order to explain these features, we examine $\nu_{\rm trans}$ and $\nu_{\rm grav}$ in detail.

We estimate the effective viscosity in wakes by using dimensional analysis. In the kinematic theory, the viscosity is given with the mean free path $l$ and the velocity dispersion $c$ as $\nu \sim cl$. Local $N$-body simulations suggest that in the wake cases, $l \sim \lambda_{\rm cr}$ and $c \sim \lambda_{\rm cr}\Omega_0$ (Salo 1995, Daisaka and Ida 1999). Then, the viscosity is

$$\nu \sim \lambda_{\rm cr}^2 \Omega_0 \sim \frac{G^2\Sigma^2}{\Omega_0^3}. \tag{25}$$

A similar result was already discussed in the gravitationally unstable systems with the linear perturbation theory. Larson (1984) estimated the gravitational torque associated with a spiral pattern and obtained $\nu_{\rm grav} \sim G^2\Sigma^2/\Omega_0^3$, using the formula given by Lynden-Bell and Kalnajs (1972) (see also Takeda and Ida 2001). Lin and Pringle (1987) also derived the effective viscosity as $\sim G^2\Sigma^2/\Omega_0^3$, considering the transport of the mass and the angular momentum similar to turbulent fluid driven by the gravitational instability. Ward and Cameron (1978) and Harris and Ward (1983) also gave the same formula, considering the energy dissipation of clumps formed by the gravitational instability within the Roche limit. With the parameters characterizing ring systems (i.e., $\tau$ and $r_h^*$), Eq. (26) is rewritten as

$$\nu \sim r_h^{*6} \tau^2 r_p^2 \Omega_0. \tag{26}$$

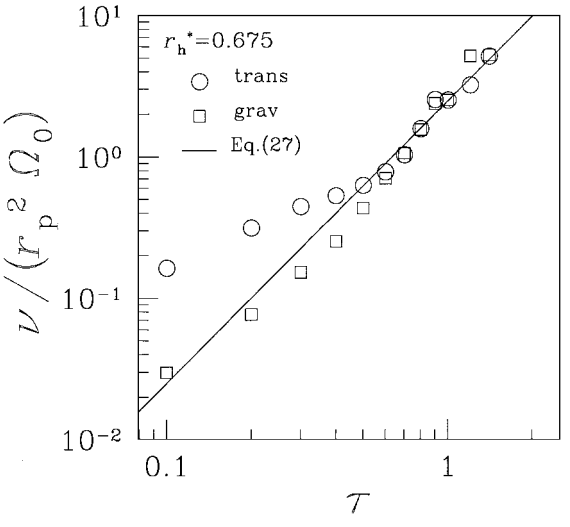


**FIG. 9.** Dependence of the translational (circles) and gravitational (squares) viscosity on $\tau$ for set (ii) (case of various values of $\tau$ with $r_h^* = 0.675$ and $\varepsilon = 0.4$). The line denotes the viscosity expected from the analytical estimation (Eq. (27)), which is proportional to $\tau^2$.

This expression would qualitatively explain the strong dependence of the viscosity on $r_h^*$ and $\tau$ in our numerical simulations with the wake structure.

In Fig 9, we plot the viscosity obtained from Eq. (27) and the results of $\nu_{\rm trans}$ and $\nu_{\rm grav}$ for set (ii), which are the same data as in Fig. 7b. In the region with wakes ($\tau \gtrsim 0.5$), $\nu_{\rm trans}$ and $\nu_{\rm grav}$ obtained from our simulations are consistent with Eq. (27). The least squares fit of our results for $\tau > 0.5$ gives the power of $\tau^2$. On the other hand, for the $r_h^*$-dependence of the viscosity, the analytical estimation does not agree with the numerical results. In Fig 10, $\nu_{\rm trans}$ and $\nu_{\rm grav}$ scaled by $1/\tau^2$ are plotted for both the numerical results and the analytical estimation. The numerical results are the same data as in Figs. 5 and 7a. The numerically obtained viscosity has a stronger dependence of $r_h^*$ than Eq. (27). The least squares fit of data for $r_h^* \geq 0.6$ yields

$$\nu_{\rm trans} \simeq \nu_{\rm grav} \simeq 190 r_h^{*11} \tau^2 \times r_p^2 \Omega_0. \tag{27}$$

Equation (28) is also expressed as

$$\nu_{\rm trans} \sim \nu_{\rm grav} \simeq \frac{1}{2} C(r_h^*) \frac{G^2\Sigma^2}{\Omega_0^3}, \tag{28}$$

where a correction factor $C$ is given by $C(r_h^*) = 26 r_h^{*5}$. For parameters corresponding to Saturn's main ring, $C$ is greater than unity (for example, $C \sim$ 6–20 for the B-ring). Since the collisional component $\nu_{\rm coll}$ is much smaller than these two components for $r_h^* > 0.7$, as shown in Fig. 7a, the total viscosity is $C G^2\Sigma^2/\Omega_0^3$ for larger $r_h^*$. A similar expression was also found in results of global $N$-body simulations performed by Takeda and Ida (2001). Note that the expression in Eq. (29) does not depend on particle sizes but only on the surface density and the distance from the center of the planet $a_0$ (see Eq. (8)). In Eq. (29), though the correction factor is included, the enhancement in the viscosity is roughly explained by the quantity $G^2\Sigma^2/\Omega_0^3$.

While gaseous disks can be infinitely compressed by the self-gravity, the compression in rings consisting of solid particles is limited. This limitation would be related to the correction factor $C$. The limitation of compression is equivalent to the limitation of the contrast in the surface density, $\Delta\Sigma$, and the magnitude of the density contrast in wakes changes with $r_h^*$. Figure 11 shows typical spatial distributions of particles obtained from two simulations with $r_h^* = 0.7$ (left panel) and $r_h^* = 0.8$ (right panel) for $\tau = 1.0$ and $\varepsilon = 0.1$. Note that in both cases, the size of computational area is $L_x = L_y = 6\lambda_{\rm cr}$. This figure clearly shows that the contrast of the wakes for $r_h^* = 0.7$ is fainter than that for $r_h^* = 0.8$; i.e., the compression is effectively suppressed due to the finite size of particles. For small $r_h^*$, such effect is significant because the physical size of particles becomes large compared with not only Hill's radius but also the typical wavelength of wakes (see Eq. (2)). Nevertheless, in the estimation of $\nu_{\rm grav}$ by Larson (1984), the density contrast $\Delta\Sigma/\Sigma$ is simply assumed to be $\Delta\Sigma/\Sigma \sim 1$ (see also Takeda and Ida 2001). Large $\Delta\Sigma$ would lead to the strong coherent motion of particles, which also enhances $\nu_{\rm trans}$. Hence the range of correction factor $C$ is likely to result mostly from the exclusion of volumes of particles due to their finite size.

We further analyze $\nu_{\rm trans}$ by splitting it into two parts. One comes from systematic bulk motion, which is defined by the velocity averaged over neighboring particles (typically, the nearest 10 particles) in the simulations. The other one comes from local random motion defined by deviation from the systematic bulk motion (Salo 1995, Daisaka and Ida 1999). These two

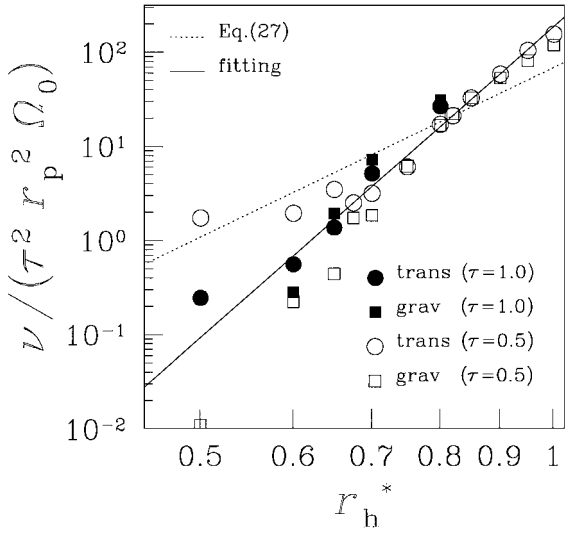


**FIG. 10.** Dependences of the translational (denoted by circles) and gravitational (squares) viscosity on $r_h^*$ for set (v) and (vi). In this figure, viscosity is also scaled by $1/\tau^2$, since scaling enables us to utilize results of simulations with different $\tau$. The dotted line is the line expected by Eq. (27), which is proportional to $r_h^{*6}$. The solid line is the line obtained by fitting data obtained by the simulations.

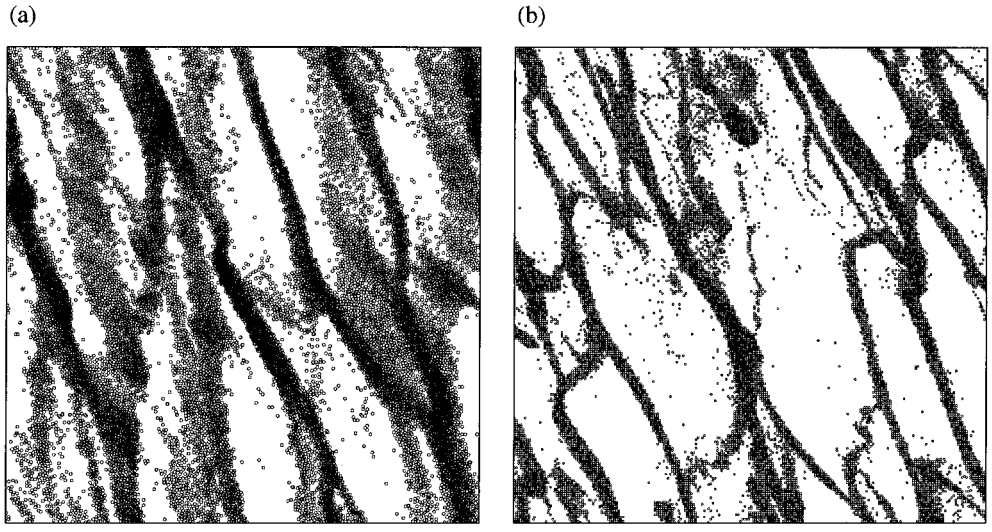


**FIG. 11.** Snapshots of particle distribution obtained from simulations for (a) $r_{\rm h}^* = 0.7$ and (b) $r_{\rm h}^* = 0.8$ with the same parameters of $\tau = 1.0$ and $\varepsilon = 0.1$. In both panels, the size of the computational area is the same ($L_x = L_y = 6\lambda_{\rm cr}$). Note that in real scale, the widths are ~310 m for $r_{\rm h}^* = 0.7$ and ~430 m for $r_{\rm h}^* = 0.8$ if we assumed $r_{\rm p} = 1$ m.

components of $\nu_{\rm trans}$ are given by

$$\begin{cases} \nu_{\rm trans,local} = \dfrac{2}{3\Omega_0 \sum_i m_i} \sum_i m_i v_{{\rm l},x,i} v_{{\rm l},y,i}, \\ \nu_{\rm trans,bulk} = \dfrac{2}{3\Omega_0 \sum_i m_i} \sum_i m_i v_{{\rm b},x,i} v_{{\rm b},y,i}, \end{cases} \tag{29}$$

where $\boldsymbol{v}_{\rm b}$ and $\boldsymbol{v}_{\rm l}$ are the bulk and the local random velocities. According the above definition, they are given by

$$\begin{cases} v_{{\rm b},x,i} = \dfrac{1}{10} \displaystyle\sum_{\substack{j \\ 10{\rm nearest}}} v_{j,x}, \\ v_{{\rm b},y,i} = \dfrac{1}{10} \displaystyle\sum_{\substack{j \\ 10{\rm nearest}}} \left( v_{j,y} + \frac{3}{2}\Omega_0 x_j \right), \end{cases} \tag{30}$$

and

$$\begin{cases} v_{{\rm l},x,i} = v_{x,i} - v_{{\rm b},x,i}, \\ v_{{\rm l},y,i} = \left( v_{y,i} + \dfrac{3}{2}\Omega_0 x_i \right) - v_{{\rm b},y,i}. \end{cases} \tag{31}$$

In the above, the term $3\Omega_0 x_i/2$ is added for the subtraction of the local shear velocity. Note that the total amount of the translational viscosity is equal to the sum of $\nu_{\rm trans,local}$ and $\nu_{\rm trans,bulk}$ (since, in $\nu_{\rm trans}$, the cross terms that consist of $v_{{\rm b},x} v_{{\rm l},y}$ and $v_{{\rm b},y} v_{{\rm l},x}$ vanish through the summation).

Salo (1995) and Daisaka and Ida (1999) showed that when the wakes are formed, the bulk velocity is strongly enhanced while the local random velocity is not. In Fig. 12, we split $\nu_{\rm trans}$ obtained in set (ii) into $\nu_{\rm trans,local}$ and $\nu_{\rm trans,bulk}$. This figure shows that the viscosity due to the bulk motion $\nu_{\rm trans,bulk}$ is dominant in large $\tau$ regions where the wake structure strongly develops, in accordance with increase in the bulk velocity $\boldsymbol{v}_{\rm b}$. On the other hand, in small $\tau$ regions, it is much smaller than the viscosity due to local random motion $\nu_{\rm trans,local}$. We also found that $\nu_{\rm trans,bulk} \gg \nu_{\rm trans,local}$ in large $r_{\rm h}^*$ where the wakes strongly develop. These results mean that the coherent motion of particles due to wakes results in a large increase in the translational viscosity and plays an important role in the angular momentum transport. Thus, the self-gravity also regulates the translational component through coherent motion induced by the gravitational instability. Takeda and Ida (2001) also did the same analysis of the translational component of the angular momentum flux and obtained the same results.

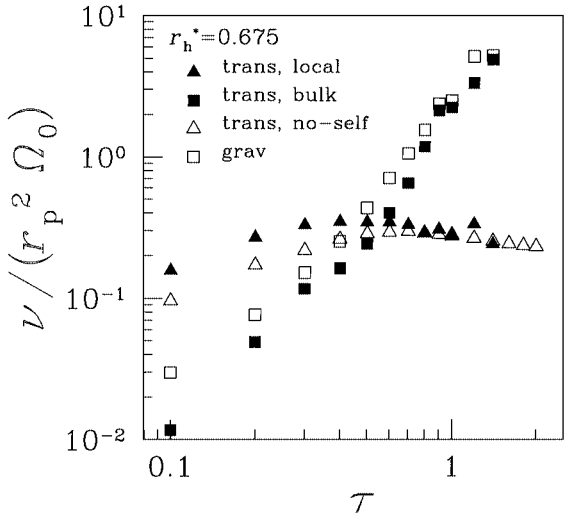


**FIG. 12.** Separation of the translational viscosity into $\nu_{\rm trans,local}$ (filled triangles) and $\nu_{\rm trans,bulk}$ (filled squares) for set (ii). Open squares denote the gravitational viscosity in this model. Open triangles express the translational viscosity obtained from simulations without self-gravity.

In Fig. 12, for comparison, we also exhibit the gravitational viscosity $\nu_{\rm grav}$ (open squares) and the translational viscosity $\nu_{\rm trans,non\text{-}grav}$ (open triangles) obtained from simulations with $r_{\rm h}^* = 0$ (non-self-gravity case). Figure 12 also shows interesting features that even in the small $\tau$ region, $\nu_{\rm grav} \simeq \nu_{\rm trans,bulk}$, and $\nu_{\rm trans,local} \simeq \nu_{\rm trans,non\text{-}grav}$ especially in the large $\tau$ region ($\tau > 0.5$). The former feature seems to be reasonable because the coherent motion is also induced by the self-gravity. The latter should indicate that self-gravity would not affect local random motion of particles because particles are densely packed as well, as in the non-self-gravitating case. In order to clarify those features, we need to perform further simulations with higher $\tau$.

## 6. SUMMARY AND DISCUSSION

We have investigated the transport process of angular momentum in a dense, self-gravitating particle system and calculated the effective viscosity by performing local $N$-body simulations where both inelastic collisions and self-gravitational interactions between particles are included. We separately calculated the translational, collisional, and gravitational viscosity directly from data of local $N$-body simulations. The first two were usually called local and non-local components of the viscosity in previous studies. Ring systems are characterized mainly by the two parameters, optical depth $\tau$ and the ratio $r_{\rm h}^*$ of Hill's radius to physical radius. The optical depth $\tau$ represents the relative importance of direct collisions to tidal effects of a central body. The ratio $r_{\rm h}^*$ is proportional to the distance from a central planet (Eqs. (8) and (9)) and expresses the relative importance of the self-gravity to the direct collisions.

The results of the numerical simulations are summarized as follows.

1. If the condition for the gravitational instability (Eq. (13)) is satisfied, for example, $\tau \gtrsim 0.5$ for $r_{\rm h}^* = 0.675$ and $r_{\rm h}^* \gtrsim 0.6$ for $\tau = 0.5$, the wake structure strongly develops because of the self-gravitational instability. The wake structure largely enhances gravitational viscosity $\nu_{\rm grav}$, and also translational viscosity $\nu_{\rm trans}$, through systematic motion associated with the wakes. Also collisional viscosity $\nu_{\rm coll}$ is enhanced due to an increase in the number of collisions in the presence of the wakes.

2. We found that, when the wake structure appears,

$$\nu_{\rm trans} \simeq \nu_{\rm grav} \gtrsim \nu_{\rm coll}. \tag{32}$$

The relative importance of $\nu_{\rm coll}$ against $\nu_{\rm trans}$ and $\nu_{\rm grav}$ is reduced as increasing $r_{\rm h}^*$. Therefore, the total viscosity is approximately given by

$$\nu_{\rm total} \simeq \nu_{\rm trans} + \nu_{\rm grav} \simeq C(r_{\rm h}^*)\frac{G^2\Sigma^2}{\Omega_0^3}, \tag{33}$$

where $C(r_{\rm h}^*) = 26 r_{\rm h}^{*5}$ is the correction factor, which may come from the effect of the finite physical size of ring particles. It takes the values of 2–6 in Saturn's C-ring, 6–20 in the B-ring, and 26–40 in the A-ring, respectively.

3. We split $\nu_{\rm trans}$ into $\nu_{\rm trans,bulk}$ due to systematic motion and $\nu_{\rm trans,local}$ due to local random motion and found $\nu_{\rm trans,bulk} \gg \nu_{\rm trans,local}$ when wake structure develops. Thus, the enhancement of $\nu_{\rm trans}$ originates from the systematic motion associated with the wakes. Both $\nu_{\rm trans,local}$ and $\nu_{\rm coll}$ are affected weakly by the wakes. When wakes do not develop ($\tau$ or $r_{\rm h}^*$ is small), dominant viscosity is $\nu_{\rm coll}$ in relatively high $\tau$ cases and $\nu_{\rm trans}$ in small $\tau$ cases, as in the non-self-gravitating cases.

The viscosity we obtained is considerably larger than the often-quoted viscosity given by Eq. (20) (Goldreich and Tremaine 1978a). Goldreich and Tremaine's formula gives $\nu \sim 0.5\ {\rm cm^2\ s^{-1}}$ for the B-ring at $\tau \sim 1.0$ and $a_0 = 1.0 \times 1.0^{10}$ cm ($\Omega_0 \sim 1.95 \times 10^{-4}\ {\rm s^{-1}}$) and $\nu \sim 0.2\ {\rm cm^2\ s^{-1}}$ for the A-ring at $\tau \sim 0.5$ and $a_0 = 1.27 \times 10^{10}$ cm ($\Omega_0 \sim 1.33 \times 10^{-4}\ {\rm s^{-1}}$), where $\sigma_r \sim r_{\rm p}\Omega_0$ and $r_{\rm p} \sim 1$m are assumed. These values are much smaller than the observationally inferred viscosity $\nu \sim 260\ {\rm cm^2\ s^{-1}}$ (Shu 1984, from density waves at Mimas 5 : 3 resonance in the mid A-ring) and $\sim 20\ {\rm cm^2\ s^{-1}}$ (Cuzzi *et al.* 1984, from the Janus 2:1 density wave in the inner B-ring). In order to explain such large values with Goldreich and Tremaine's viscosity, Shu (1984) suggested that the random velocity of particles is largely enhanced by the density waves due to satellite gravity. The estimated velocity is $\sim 30 r_{\rm p}\Omega_0$, which is much larger than the expected equilibrium velocity due to mutual collisions of particles ($\sim r_{\rm p}\Omega_0$), and such large random velocity would suppress the wake formation since it leads to $\mathcal{Q} > 2$. Our result gives $\nu \sim 60\ {\rm cm^2\ s^{-1}}$ for the B-ring and $\nu \sim 100\ {\rm cm^2\ s^{-1}}$ for the A-ring, where we assume that $\Sigma = 100\ {\rm g\ cm^{-2}}$ for the B-ring and $\Sigma = 40\ {\rm g\ cm^{-2}}$ for the A-ring (Esposito 1993). Our estimations are comparable to those observationally inferred values. Salo (1995) also estimated the enhanced viscosity by taking into account the strong increase in the radial velocity dispersion due to the wake formation, but by using Goldreich and Tremaine's viscosity. However, such estimation is not appropriate in the case with wakes, as shown in the present study.

The large viscosity accelerates the viscous evolution of the ring. Our formula predicts that the diffusion time of a ringlet with width $\Delta r$ is

$$\Delta t = \frac{(\Delta r)^2}{\nu} \simeq 5 \times 10^4 \left(\frac{a_0}{1.0 \times 10^{10}\ {\rm cm}}\right)^{-19/2} \times \left(\frac{\Sigma}{100\ {\rm g\ cm^{-2}}}\right)^{-2} \left(\frac{\Delta r}{100\ {\rm km}}\right)^2 [y], \tag{34}$$

where we assumed that mass is $M_{\rm s} = 5.68 \times 10^{29}$ g and material density is $\rho = 0.9\ {\rm g\ cm^{-3}}$. For a ringlet with width 100 km, the estimated diffusion time is only $5 \times 10^4$ years, so that the observed ringlet structure with typical scale width $\sim$100 km should be made by a formation process on a timescale $\lesssim 10^4$–$10^5$ years. Note that the wake structure we found has a typical scale $\sim$100 m, and the ringlet structure is much larger than the wakes.

The proposed formation models for the ringlet structures in Saturn's ring require a characteristic property of the viscosity. The viscous instability model (Lin and Bodenheimer 1981,

Lukkari 1981, Ward 1981) requires $\partial(\Sigma\nu)/\partial\Sigma < 0$ (equivalently, $\partial(\tau\nu)/\partial\tau < 0$). However, the results in non-self-gravitating cases showed that $\nu$ is an only increasing function with respect to $\tau$, so that $\partial(\tau\nu)/\partial\tau > 0$ (e.g., Fig. 4 and Araki and Tremaine 1986, Wisdom and Tremaine 1988). Figure 6 shows that, also in the self-gravitating cases, $\partial(\tau\nu)/\partial\tau > 0$ as well. Hence the viscous instability is not probable even if the effect of the self-gravity is taken into account.

Another model proposed to explain the ringlet structure is the viscous overstability model (Borderies *et al*. 1985, Schmit and Tscharnuter 1995). By performing local simulations, Mosqueira (1996) gave an indirect evidence for the instability in perturbed rings. Recently, Salo *et al*. (submitted) demonstrated the viscous overstability rather directly, in which the growth of density contrast parallel to the azimuthal direction (i.e., axisymmetrical structure) could be recognized in the spatial distributions of particles. Schmit and Tscharnuter (1995) developed linear stability analysis in self-gravitating, viscous fluid and obtained the dispersion relation. For the viscosity in the form as $\nu \propto \Sigma^{\beta}$, they showed that if the constant $\beta$ is sightly larger than zero, overstability occurs. Salo *et al*. (submitted) also obtained the condition as $\beta \gtrsim 1$ from results of their simulations. Our obtained viscosity gives $\beta \approx 2$ which exceeds both conditions by a large margin, so that the viscosity we found satisfies the condition of overstability. Actually, as well as Salo *et al*. (submitted), our simulation for $\tau = 1.0$, $r_{\rm h}^{*} = 0.5$, $\varepsilon =$

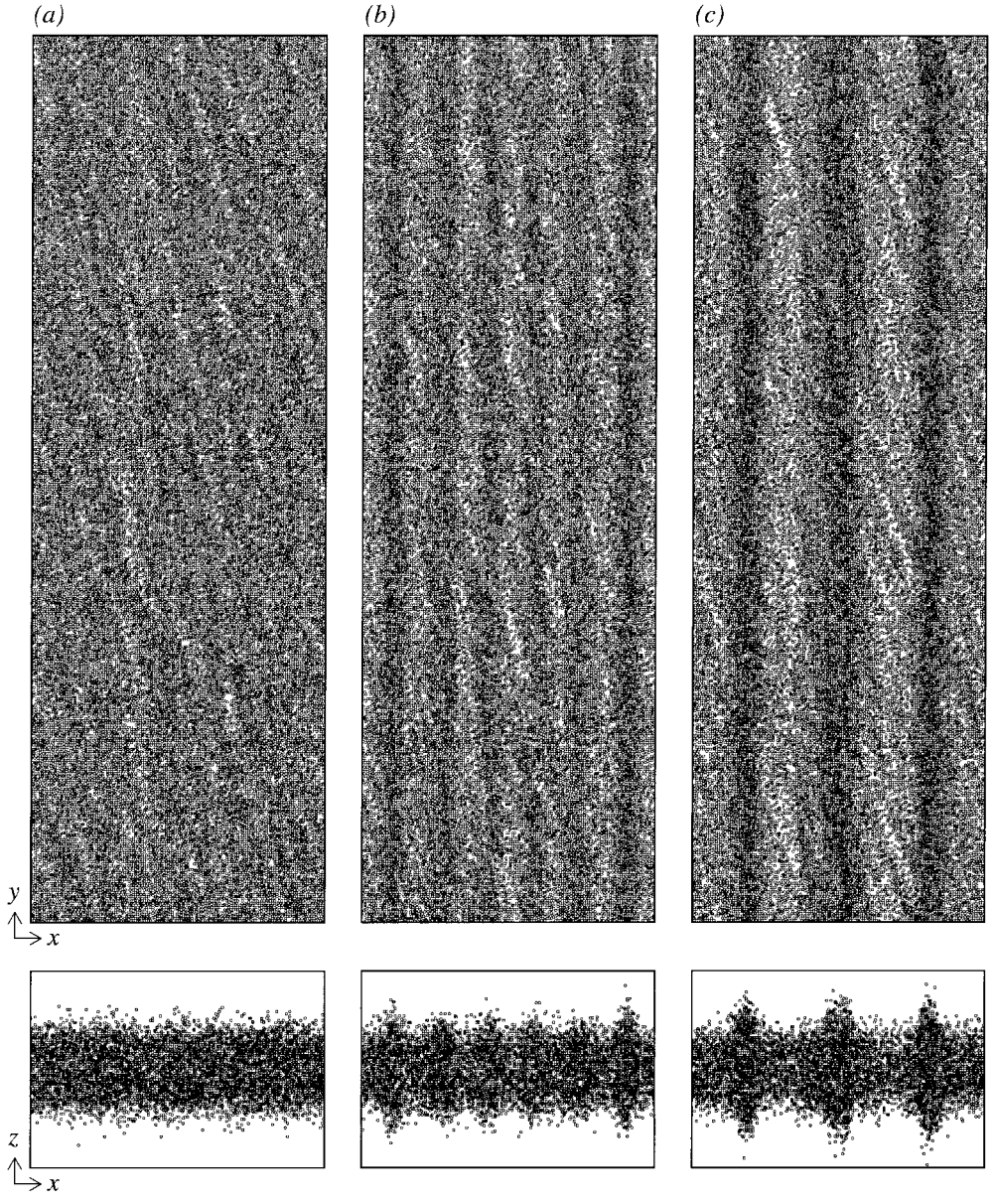


**FIG. 13.** Spatial distributions of particles at (a) $t = 16\,t_{\rm K}$, (b) $t = 40\,t_{\rm K}$, and (c) $t = 66\,t_{\rm K}$, obtained from a simulation with $\tau = 1.0$, $r_{\rm h}^{*} = 0.5$, $\varepsilon = 0.5$. The size of a simulation cell is set as $12\lambda_{\rm cr} \times 36\lambda_{\rm cr}$ ($N = 48{,}858$). Upper and lower panels are face-on and edge-on views, respectively. Note that in the edge-on view, the distributions are expanded along the $z$-direction to emphasize splashing of particles.

0.1 exhibited signs of overstability, as shown in Fig. 13. From this figure, the growth of the overstability could be seen: at $t = 16\,t_{\rm K}$, density contrast could not be recognized yet; then it seems to emerge at $t = 40\,t_{\rm K}$ and becomes clearer at $t = 66\,t_{\rm K}$. Such a density pattern develops with time. Time required for the growth of the overstability is much larger than the characteristic time for the gravitational instability ($\sim$few $t_{\rm K}$). The edge-on views in Fig. 13 show vertical splashing of particles at positions that correspond to the denser parts in the face-on views, which was supposed by Borderies *et al*. (1985) and also was demonstrated by Salo *et al*. (submitted). To follow the growth of the overstability into a non-linear regime, Schmit and Tscharnuter (1999) numerically solved the hydrodynamical equations and suggested that large-scale surface density fluctuation with 10–15 km emerges on a timescale of 10 years at the location of the B-ring, which is shorter than the diffusion time for a ringlet with 10 km ($5 \times 10^2$ years). Thus, the viscous overstability may be a good candidate to explain the ringlet structure but more detailed simulations would be necessary.

The moonlet hypothesis is also proposed for the explanation of the ringlets, in which a gap is created by gravitational scatterings of embedded large particles (moonlets) against viscous diffusion (Hénon 1981). Spahn (1987) compared synodic time of a moonlet with viscous diffusion time with viscosity of Eq. (20). More exactly, the gravitational torque generated by gravitational scattering of a moonlet must be compared with viscous torque. In this way, Lin and Papaloizou (1973, 1993) derived the condition of gap opening as

$$\left(\frac{M_{\rm m}}{M_{\rm s}}\right) \gtrsim 40\left(\frac{\nu}{a_0^2\Omega_0}\right). \tag{35}$$

This expression shows that a larger mass of a moonlet is needed to open up a gap in a system with larger viscosity. A similar estimation was made by Petit and Hénon (1987b, 1988), in which they used the observed value of the viscosity by Voyager. From Eq. (36), for the B-ring ($a_0 = 1.0 \times 10^{10}$ cm, $M_{\rm s} = 5.68 \times 10^{29}$ g, and $\Omega_0 = 1.95 \times 10^{-4}$ s$^{-1}$), the moonlet mass necessary to open up a gap is estimated as $\gtrsim 6 \times 10^{14}$ g with the viscosity of Eq. (20) ($\nu = 0.5$ cm$^2$ s$^{-1}$), while $\gtrsim 7 \times 10^{16}$ g with our result ($\nu = 60\,{\rm cm^2 s^{-1}}$). By assuming material density $\rho = 0.9\,{\rm g\,cm^{-3}}$, the radius of the moonlet is $\sim$0.5 and $\sim$3 km for the individual viscosity. Our viscosity requires a much larger size of a moonlet for gap creation and such a moonlet in the Saturn's main ring would be discovered by the Cassini mission if it exists.

## APPENDIX: DERIVATION OF GRAVITATIONAL VISCOSITY IN HILL'S COORDINATE SYSTEM

In this appendix, we derive gravitational viscosity $\nu_{\rm grav}$ in Eq. (19), which is the formula in Hill's coordinate system in particle image. According to Takeda and Ida (in press), in cylindrical coordinates ($r$, $\theta$, $z$), angular momentum flux $\Phi_{\rm grav}$ due to self-gravitational torque, averaged over radial range $[r_0,\ r_0 + \Delta_r]$, is

$$\overline{\Phi_{\rm grav}} = \frac{1}{\Delta r}\int_{r_0}^{r_0+\Delta r} dr \int_{r_{\rm min}}^{r} dr' \int_0^{2\pi} r'\,d\theta' \int_{-\infty}^{\infty} dz'\rho(\boldsymbol{r}')\frac{\partial \varphi_{\rm self}}{\partial \theta'}(\boldsymbol{r}'), \tag{37}$$

where $\varphi_{\rm self}$ is the self-gravitational potential. Substituting Eq. (16) into Eq. (37) and adopting Hill's approximation, we reduce Eq. (37) to

$$\overline{\Phi_{\rm grav}} \simeq -2\pi r_0^2 G \frac{1}{L_x L_y}\int_{-L_x/2}^{L_x/2} dx \frac{1}{L_y}\int_{-L_y/2}^{L_y/2} dy' \int_{x_{\rm min}}^{x} dx' \int_{-\infty}^{\infty} dz' \times \int_{x}^{x_{\rm max}} dx'' \int_{y_{\rm min}}^{y_{\rm max}} dy'' \int_{-\infty}^{\infty} dz''\rho(\boldsymbol{x}')\rho(\boldsymbol{x}'')\frac{y''-y'}{|\boldsymbol{x}''-\boldsymbol{x}'|^3}, \tag{38}$$

where we used approximations for integrals in terms of $r$ and $\theta$ as

$$\begin{cases} \dfrac{1}{\Delta r}\displaystyle\int_{r_0}^{r_0+\Delta_r} dr \simeq \frac{1}{L_x}\int_{-L_x/2}^{L_x/2} dx, \\ \dfrac{1}{2\pi r}\displaystyle\int_0^{2\pi} r\,d\theta \simeq \frac{1}{L_y}\int_{-L_y/2}^{L_y/2} dy, \end{cases} \tag{39}$$

where $L_x$ and $L_y$ are sizes of a computational area. In particle image, $\rho(\boldsymbol{x})$ is also expressed by using Dirac's $\delta$-function as

$$\rho(\boldsymbol{x}') = \sum_i m_i \delta(\boldsymbol{x}' - \boldsymbol{x}_i). \tag{40}$$

Substituting Eq. (40) into Eq. (38) yields

$$\overline{\Phi_{\rm grav}} = \frac{-G}{L_x}\int_{-L_x/2}^{L_x/2} dx \frac{1}{L_y}\sum_{\substack{i \\ x_i<x}}\sum_{\substack{j \\ x_j>x}} m_i m_j \frac{y_j - y_i}{|\boldsymbol{x}_j - \boldsymbol{x}_i|^3}. \tag{41}$$

The integrand in Eq. (41) has a no-zero value for $x_i < x < x_j$ so that

$$\sum_{\substack{i \\ x_i<x}}\sum_{\substack{j \\ x_j>x}} m_i m_j \frac{y_j - y_i}{|\boldsymbol{x}_j - \boldsymbol{x}_i|} = \sum_i \sum_{\substack{j \\ x_j>x_i}} m_i m_j \frac{y_j - y_i}{|\boldsymbol{x}_j - \boldsymbol{x}_i|^3}\Theta(x; x_i, x_j), \tag{42}$$

where

$$\Theta(x; x_i, x_j) = \begin{cases} 1 & x_i < x < x_j, \\ 0 & \text{otherwise.} \end{cases} \tag{43}$$

Then,

$$\overline{\Phi_{\rm grav}} = \frac{-2\pi r_0^2 G}{L_x L_y}\sum_i \sum_{\substack{j \\ x_j>x_i}} m_i m_j \frac{(y_j - y_i)(x_j - x_i)}{|\boldsymbol{x}_j - \boldsymbol{x}_i|^3}. \tag{44}$$

With Eq. (18), the expression of $\nu_{\rm grav}$ in Eq. (19) is obtained.

## ACKNOWLEDGMENTS

The authors thank Heikki Salo and an anonymous referee for their useful comments and suggestions to improve the manuscript. We are indebted to Keiji Ohtsuki for useful advice and to Takaaki Takeda for useful discussions.

## REFERENCES

Anthony, D. M., and R. G. Carlberg 1988. Spiral wave viscosity in self-gravitating accretion disks. *Astrophys. J.* **332**, 637–645.

Araki, S., and S. Tremaine 1986. The dynamics of dense particle disk. *Icarus* **65**, 83–109.

Borderies, N., P. Goldreich, and S. Tremaine 1985. A granular flow model for dense planetary rings. *Icarus* **63**, 406–420.

Bridges, F. G., A. Hatzed, and D. N. C. Lin 1984. Structure, stability and evolution of Saturn's rings. *Nature* **309**, 333–335.

Cameron, A. G. W., and W. R. Ward 1976. The origin of the Moon. *Lunar Sci. Abs.* **7**, 120–122.

Canup, R. M., and L. W. Esposito 1995. Accretion in the Roche zone: Coexistence of rings and ringmoons. *Icarus* **113**, 331–352.

Cuzzi, J. N., J. J. Lissauer, L. W. Esposito, J. B. Holberg, E. A. Marouf, G. L. Tyler, and A. Boischot 1984. Saturn's rings: Properties and processes. In *Planetary Rings* (R. Greenberg and A. Brahic, Eds.), pp. 73–199. Univ. of Arizona Press, Tucson.

Daisaka, H., and S. Ida 1999. Spatial structure and coherent motion in dense planetary rings induced by self-gravitational instability. *Earth, Planet Space* **51**, 1195–1213.

Dilley, J. P. 1993. Energy loss in collisions of icy spheres: Loss mechanism and size–mass dependence. *Icarus* **105**, 225–234.

Dones, L., J. N. Cuzzi, and M. R. Showalter 1993. Voyager photometry of Saturn's A ring. *Icarus* **105**, 184–215.

Esposito, L. W. 1993. Understanding planetary rings. *Annu. Rev. Earth Planet. Sci.* **21**, 487–523.

Franklin, F. A., A. F. Cook II, R. T. F. Barrey, C. A. Roff, and G. E. Hunt 1987. Voyager observations of the azimuthal brightness variations in Saturn's rings. *Icarus* **69**, 280–296.

Goldreich, P., and S. Tremaine 1978a. The velocity dispersion in Saturn's rings. *Icarus* **34**, 227–239.

Goldreich, P., and S. Tremaine 1978b. The formation of the Cassini division in Saturn's rings. *Icarus* **34**, 240–253.

Goldreich, P., and S. Tremaine 1982. The dynamics of planetary rings. *Annu. Rev. Astron. Astrophys.* **20**, 249–283.

Greenberg, R. 1988. Particle properties and the large-scale structure of planetary rings: Rebound characteristics and viscosity. *Icarus* **75**, 527–539.

Harris, W. R., and A. W. Ward 1983. On the radial structure of planetary rings. In *Proceedings of I.A.U. Colloquium 75 Planetary Rings, Toulouse, France, August 1982*. (A. Brahic, Ed.).

Hartmann, W. K., and D. R. Davis 1975. Satellite-sized planetesimals and lunar origin. *Icarus* **24**, 504–515.

Hatzes, A. P., F. G. Bridges, and D. N. C. Lin 1988. Collisional properties of ice spheres at low impact velocites. *Mon. Not. R. Astron. Soc.* **231**, 1091–1115.

Hénon, M. 1981. A simple model of Saturn's rings. *Nature* **293**, 33–35.

Hill, G. W. 1878. Researches in the lunar theory. *Amer. J. Math.* **1**, 5–26, 129–147, 245–260.

Ida, S., R. M. Canup, and G. R. Stewart 1997. Lunar accretion from an impact-generated disk. *Nature* **389**, 353–357.

Julian, W. H., and A. Toomre 1966. Non-axisymmetrical responses of differentially rotating disks of stars. *Astrophys. J.* **146**, 810–827.

Kokubo, E., J. Makino, and S. Ida 2000. Evolution of a circumterrestrial disk and formation of a single moon. *Icarus* **148**, 419–436.

Larson, R. B. 1984. Gravitational torques and star formation. *Mon. Not. R. Astron. Soc.* **206**, 197–207.

Laughlin, G., and P. Bodenheimer 1994. Nonaxisymmetric evolution in protostellar disks. *Astrophys. J.* **436**, 335–354.

Laughlin, G., and M. Rozyczka 1996. The effect of gravitational instabilities of protostellar disks. *Astrophys. J.* **456**, 279–291.

Lin, D. N. C., and P. Bodenheimer 1981. On the stability of Saturn's rings. *Astrophys. J.* **248**, L83–L86.

Lin, D. N. C., and J. C. B. Papaloizou 1979. Tidal torques on accretion discs in binary systems with extreme mass ratios. *Mon. Not. R. Astron. Soc.* **1979**, 799–812.

Lin, D. N. C., and J. C. B. Papaloizou 1993. On the tidal interaction between protostellar disks and companions. In *Protostar and Planet III* (E. H. Levy and J. I. Lunine, Eds.), pp. 749–836. Univ. of Arizona Press, Tucson.

Lin, D. N. C., and J. E. Pringle 1987. A viscosity prescription for a self-gravitating accretion disc. *Non. Not. R. Astron. Soc.* **225**, 607–613.

Lukkari, J. 1981. Collisional amplification of density fluctuations in Saturn's rings. *Nature* **292**, 433–435.

Lynden-Bell, D., and A. J. Kalnajs 1972. On the generating mechanism of spiral structure. *Mon. Not. R. Astron. Soc.* **157**, 1–30.

Lynden-Bell, D., and F. E. Pringle 1974. The evolution of viscous discs and the origin of the nebular variables. *Mon. Not. R. Astron. Soc.* **168**, 603–637.

Makino, J., and S. J. Aarseth 1992. On a hermite integrator with Ahmad–Cohen scheme for gravitational many-body problems. *Publ. Astron. Soc. Jpn.* **44**, 141–151.

Makino, J., E. Kokubo, and M. Taiji 1993. HARP: A special-purpose computer for $N$-body problem. *Publ. Astron. Soc. Jpn.* **45**, 349–360.

Mosqueira, I. 1996. Local simulation of perturbed dense planetary rings. *Icarus* **122**, 128–152.

Nakazawa, K., and S. Ida 1988. Hill's approximation in the three-body problem. *Prog. Theoret. Phys. Suppl.* **96**, 167–174.

Ohtsuki, K. 1993. Capture probability of colliding planetesimals: Dynamical constraints on accretion of planets, satellites, and ring particles. *Icarus* **106**, 228–246.

Ohtsuki, K. 1999. Evolution of particle velocity dispersion in a circumplanetary disk due to inelastic collisions and gravitational interactions. *Icarus* **137**, 152–177.

Ohtsuki, K., and H. Emori 2000. Local $N$-body simulations for the distribution and evolution of particle velocities in planetary rings. *Astron. J.* **119**, 403–416.

Petit, J.-M., and R. Greenberg 1996. Viscosity in Keplerian disks: Steady-state velocity distribution and non-local collision effects. *Icarus* **123**, 524–535.

Petit, J.-M., and M. Hénon 1986. Satellite encounters. *Icarus* **66**, 536–555.

Petit, J.-M., and M. Hénon 1987a. A numerical simulation of planetary rings I. Binary encounters. *Astron. Astrophys.* **173**, 389–404.

Petit, J.-M., and M. Hénon 1987b. A numerical simulation of planetary rings II. Monte Carlo model. *Astron. Astrophys.* **188**, 198–205.

Petit, J.-M., and M. Hénon 1988. A numerical simulation of planetary rings III. Mass segregation, ring confinement, and gap formation. *Astron. Astrophys.* **199**, 343–356.

Richardson, D. C. 1994. Tree code simulations of planetary rings. *Mon. Not. R. Astron. Soc.* **269**, 493–511.

Salo, H. 1991. Numerical simulations of dense collisional systems. *Icarus* **90**, 254–270.

Salo, H. 1992a. Numerical simulations of dense collisional systems. II. Extended distribution of particle sizes. *Icarus* **96**, 85–106.

Salo, H. 1992b. Gravitational wakes in Saturn's rings. *Nature* **395**, 619–621.

Salo, H. 1995. Simulations of dense planetary rings. III. Self-gravitating identical particles. *Icarus* **117**, 287–312.

Salo, H., J. Schmidt, and F. Spahn (2001). Viscous overstability in Saturn's B-ring: I. Direct simulations and measurement of transport coefficients. *Icarus* **153**, 295–315.

Schmit, U., and W. M. Tscharnuter 1995. A fluid dynamical treatment of the common action of self-gravitation, collision, and rotation in Saturn's B-Ring. *Icarus* **115**, 304–319.

Schmit, U., and W. M. Tscharnuter 1999. On the formation of the fine-scale structure in Saturn's B ring. *Icarus* **138**, 173–187.

Shu, F. H. 1984. Waves in planetary rings. In *Planetary Rings* (R. Greenberg and A. Brahic, Eds.), pp. 513–561. Univ. of Arizona Press, Tucson.

Spahn, F. 1987. Scattering properties of a moonlet (satellite) embedded in a particle ring: Application to the rings of Saturn. *Icarus* **71**, 69–77.

Takeda, T., and S. Ida 2001. Angular momentum transfer in a protolunar disk. *Astrophys. J.* **560**, 514–533.

Toomre, A. 1964. On the gravitational instability of a disk of stars. *Astrophys. J.* **139**, 1217–1238.

van der Tak, F., I. de Peter, A. Silva, and R. Millan 1999. Time variability in the radio brightness distribution of Saturn. *Icarus* **142**, 125–147.

Ward, W. R. 1981. On the radical structure of Saturn's ring. *Geophys. Res. Lett.* **8**, 641–643.

Ward, W. R., and A. G. W. Cameron 1978. Disc evolution within the Roche limit. In *Proc. Lunar Planet. Sci. Conf.*, p. 1205 (abstract IX).

Wisdom, J., and S. Tremaine 1988. Local simulation of planetary rings. *Astron. J.* **95**, 925–940.